Addressing Challenges of Volume Controlled Cavity Expansion (VCCE) for In-Vivo Tissue Testing

by

Katherine Charlotte Spaeth

B.S., Environmental Engineering, North Carolina State University (2017)

Submitted to the Department of Mechanical Engineering
in partial fulfillment of the requirements for the degrees of

NAVAL ENGINEER'S DEGREE

and

MASTER OF SCIENCE IN MECHANICAL ENGINEERING

at the

MASSACHUSETTS INSTITUTE OF TECHNOLOGY

May 2024

Author: Katherine Charlotte Spaeth
Department of Mechanical Engineering
May 10, 2024

Certified by: Tal Cohen
Associate Professor of Mechanical Engineering
Associate Professor of Civil and Environmental Engineering
Thesis Supervisor

Accepted by: Nicolas Hadjiconstantinou
Chairman, Department Committee on Graduate Theses

Addressing Challenges of Volume Controlled Cavity Expansion (VCCE) for In-Vivo Tissue Testing

by
Katherine Charlotte Spaeth

Submitted to the Department of Mechanical Engineering
on May 10, 2024, in partial fulfillment of the
requirements for the degrees of
NAVAL ENGINEER'S DEGREE
and
MASTER OF SCIENCE IN MECHANICAL ENGINEERING

Abstract

The prevalence of Traumatic Brain Injuries (TBI's) is a serious health concern to U.S. Military Members. Mild TBI's, some of which have been shown to result from prolonged exposure to repeated artillery blasts, are particularly challenging to identify with existing diagnostic imaging technology. In general, as with other soft-tissued organs, there exists a gap in understanding of how biological tissues deform under extreme loading conditions. Understanding these mechanics has applications beyond diagnosing physical bodily injuries as diseased tissues have also been shown to demonstrate differing mechanical properties. Volume Controlled Cavity Expansion (VCCE) is a novel, needle-based probing methodology developed to capture rate dependent ex-vivo and in-vivo tissue material properties. In this thesis, the VCCE methodology was performed on numerous animal tissues as well as extracted human thyroids to study some of the challenges related to the translation of the VCCE lab technique into a medical diagnostics tool. To ensure a successful VCCE test, it was shown that choice of needle and the insertion protocol must be altered depending on the type of biological tissue being tested. Additionally, in a clinic setting, VCCE was demonstrated as a successful methodology in differentiating between a diseased and healthy tissue. Using the mechanics-informed in-vivo tissue probing method, VCCE has applications for improved assessment and diagnostic tools for injured and/or diseased tissues, Personal Protective Equipment (PPE), and casualty transport safety guidelines.

Thesis Supervisor: Tal Cohen
Title: Associate Professor of Mechanical Engineering
Associate Professor of Civil and Environmental Engineering

Acknowledgments

Firstly, I want to thank my thesis Advisor Dr. Tal Cohen for her guidance and support during the duration of this work. She has cultivated an environment of dedicated, curious, and cooperative students who truly made me feel like a part of the team.
To Dr. Cohen's Nonlinear Solid Mechanics Group, especially Hannah Varner and Brendan Unikewicz, thank you so much for your patience in teaching me most of the background behind this project and providing consistent insight while I was conducting my experiments.
Lastly, thank you to my parents and other family members, boyfriend, and 2N cohort for providing the moral support required to complete this work.

Contents

List of Figures

List of Tables

Chapter 1

Introduction

Traumatic Brain Injury (TBI)'s remain a significant health concern to U.S. military members. From 2010 to 2014, an estimated 135,235 service members suffered some form of a TBI, in particular, the U.S. Navy and U.S Marine Corps composed approximately 25% of these reported injuries [1]. The consequences of such injuries can result in long-term cognitive issues, emotional disregulation and behavioral changes as well as losses in motor functionality [2]. Not only is the prevalence of TBI injuries concerning but additional soft-tissued organs can undergo similiar extreme loading scenarios while Sailors and Marines are conducting any number of routine operations.

Diagnosing compromised soft-tissues in a ship setting or battlefield is a particularly time-sensitive and resource limited challenge. TBI injuries, especially those considered mild, are notably difficult to identify with current medical imaging tools. This can be partially attributed to the gap in understanding the mechanisms by which biological tissues deform under extreme loading conditions. Understanding the behavior of materials under such circumstances could allow for assessment and diagnosis of damaged tissues as well as the development of improved, Personal Protective Equipment (PPE) and casualty transport safety guidelines. This type of research is also relevant to the human engineering of safer Naval asset operating environments.

Similar to a physically damaged tissue, diseased tissues have also been shown to display different mechanical properties depending on the type and/or severity of disease. Cancer, for example, can involve the growth of nodules which significantly impact the surrounding micro-environment. As the abnormal group of cells proliferate, mechanical characteristics of the tissue such as solid stiffness can be altered. Advancements in research connecting the mechanical properties of a compromised tissue to an associated disease could help improve the accuracy of many current diagnostic practices as well as provide new pathways for disease treatment methods.

Utilizing a novel, needle-based probing methodology known as Volume Controlled Cavity Expansion (VCCE), Dr. Cohen's lab is developing a material testing method that could be used to capture rate dependent ex-vivo and in-vivo tissue properties. Prior VCCE experiments have been limited in scope; primarily consisting of using a large, non-portable testing set-up to probe synthetic materials that simulate biological tissue behavior or limited biological samples such as animal brain tissue and blood clots. The purpose of this thesis is to address some of the challenges related to the

translation of the VCCE lab technique into a medical diagnostics tool.

1.1 Motivation

1.1.1 Traumatic Injury Diagnostic Practices in the U.S. Navy

Modern U.S. Naval Warships pose a multitude of non-combat occupational hazards, of which bodily blunt force trauma injuries are among the most common mechanisms of harm (Figure 1-1). From everyday movements, such as climbing up steep ladderwells to access each deck or ship level, to weekly Replenishment at Sea (RAS) operations where Sailors orchestrate the movement of pallets on high tensioned wire ropes connected to the Replenishment ship, pieces of equipment and machinery found on warships can be very heavy, move at high rates of speed and/or utilize highly pressurized fluids to operate (Figure 1-2). In times of conflict, these trauma-related injuries and deaths can only be expected to increase.

TABLE 1. Top 15 Noncombat Surface and Submarine Causes of Injury or Death 1970–2020

Injury Mechanism	Casualties (n)	Mortality (%)	Most Recent Occurrence
Fire/burn/smoke inhalation injury (103 events)	923	13	2018
Man overboard (220 events)	352	71.9	2018
Collision (14 events)	275	40.3	2017
Extremity amputation, crush, or laceration	223	0	2019
Blunt torso/chest trauma	153	26.1	2018
Explosion (16 events)	106	60.4	2003
Chemical exposure/inhalation injury (27 events)	104	27.9	2004
Fall from height (other than man overboard)	75	59.2	2020
Blunt head/neck trauma	34	73.5	2005
Electrocution	32	90.6	2018
Ordinance-related mishap	24	37.5	2004
Eye trauma	17	0	2018
Cardiac arrest	17	100	2015
Suicide	12	91.7	2018
Accidental discharge (gunshot wound)	8	75	2004

Figure 1-1: Top 15 Noncombat Surface and Submarine Causes of Injury or Death 1970-2020 [3]

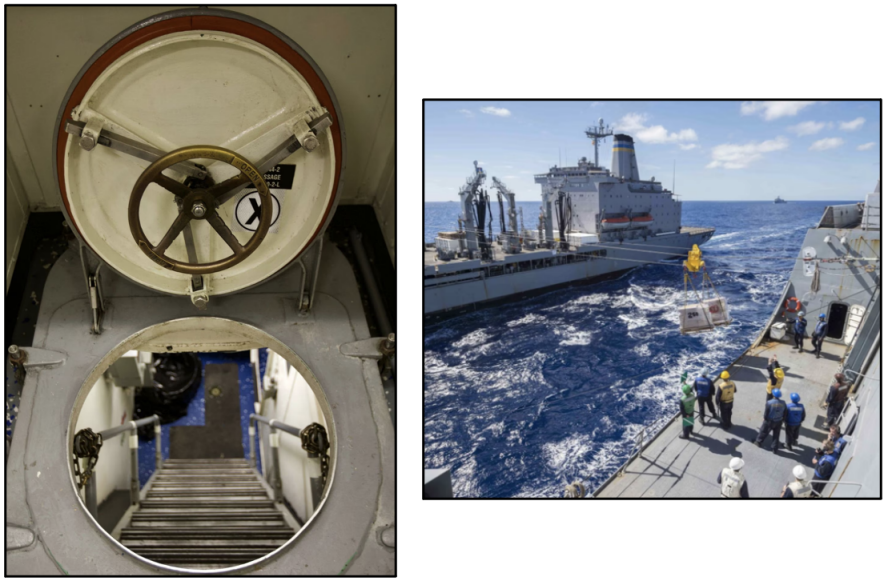

Figure 1-2: U.S. Navy Ship Ladderwell and Hatch (L) and RAS Operations (R)

Blunt force injuries occur when the body is impacted forcefully. Depending on the severity, speed, and length of time of the object's impact as well as the contact area and tissue elasticity, superficial injuries and/or damage to bones (fractures) and internal organs (contusions and lacerations) can result [4]. Some blunt impact injuries are physically apparent immediately after occurrence but deeper injuries may take days to weeks to manifest. TBI's are among the least well understood traumatic injuries due to the large range of symptomatic outcomes, developing pathology, and long term degenerative diseases [5].

All branches of the U.S. Military currently utilize the Military Acute Concussion Evaluation (MACE)-2 tool for assessment and diagnosis of suspected traumatic brain injuries [6]. This tool depends mostly on the Sailor or Solider self-reporting on the description of the event leading to the injury, observing outward physical signs of abnormal behaviors as well as a brief neurological and cognitive exam (see Figure 1-3). A concussion management tool will provide recommendations based on the MACE-2 results for further assessment and guidance, such as a Computed Tomography (CT) scan. However, for the case of mild Traumatic Brain Injury (mTBI)'s where physical evidence of damage to the head or brain is typically absent, a CT or Magnetic Resonance Imaging (MRI) may not be able to detect all types of compromised brain tissue such as when changes in microstructural of white matter or fiber tract integrity is compromised [7].

In the mid to late 2010's, Soldiers serving in Syria, Iraq and Afghanistan were suspected to have suffered countless mTBI's as a result of sustained exposure to soundwaves generated by the launching of hundreds of rockets and artillery guns in a condensed time period [9],[7]. In these cases, many soldiers were diagnosed with chronic traumatic encephalopathy where symptoms include behavioral changes, memory loss, and cognitive impairments which can progressively worsen over decades [7]. Indeed,

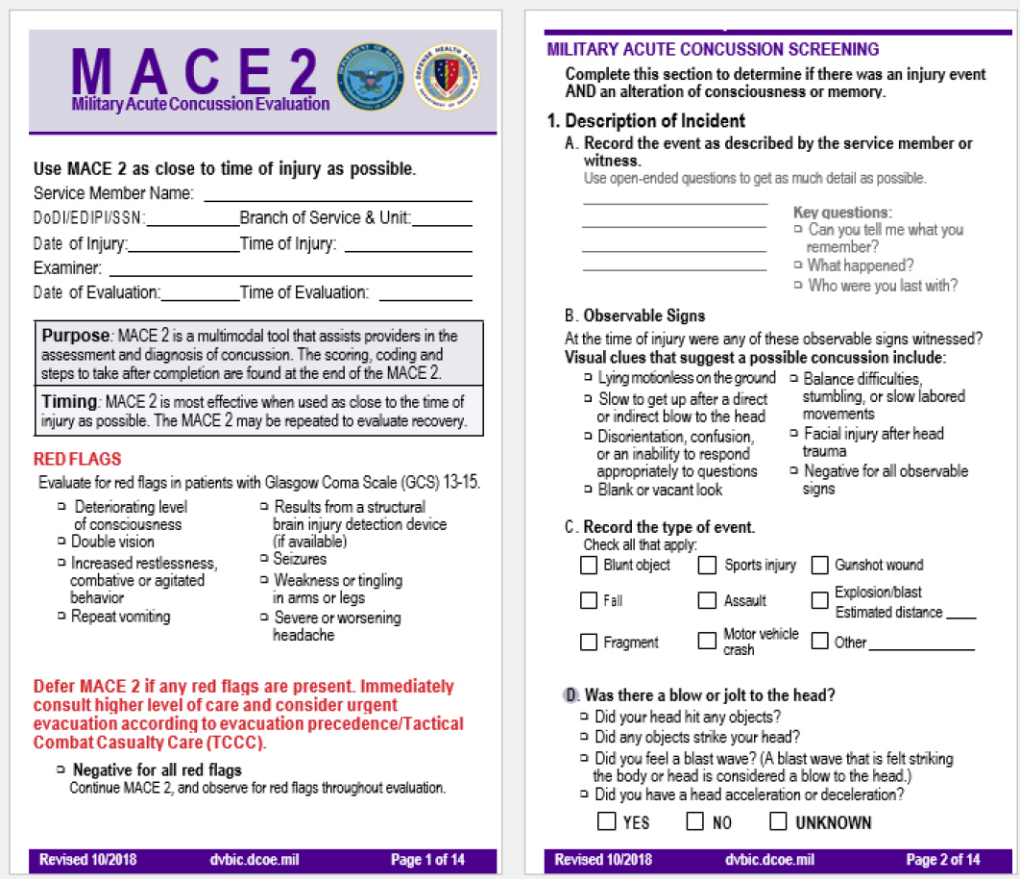

MACE 2
Military Acute Concussion Evaluation

Use MACE 2 as close to time of injury as possible.
Service Member Name: _____
DoDI/EDIPI/SSN: _____ Branch of Service & Unit: _____
Date of Injury: _____ Time of Injury: _____
Examiner: _____
Date of Evaluation: _____ Time of Evaluation: _____

Purpose: MACE 2 is a multimodal tool that assists providers in the assessment and diagnosis of concussion. The scoring, coding and steps to take after completion are found at the end of the MACE 2.

Timing: MACE 2 is most effective when used as close to the time of injury as possible. The MACE 2 may be repeated to evaluate recovery.

RED FLAGS
Evaluate for red flags in patients with Glasgow Coma Scale (GCS) 13-15.

- Deteriorating level of consciousness
- Double vision
- Increased restlessness, combative or agitated behavior
- Repeat vomiting
- Results from a structural brain injury detection device (if available)
- Seizures
- Weakness or tingling in arms or legs
- Severe or worsening headache

Defer MACE 2 if any red flags are present. Immediately consult higher level of care and consider urgent evacuation according to evacuation precedence/Tactical Combat Casualty Care (TCCC).

- **Negative for all red flags**
  Continue MACE 2, and observe for red flags throughout evaluation.

Revised 10/2018 dvbic.dcoe.mil Page 1 of 14

MILITARY ACUTE CONCUSSION SCREENING

Complete this section to determine if there was an injury event AND an alteration of consciousness or memory.

1. Description of Incident

A. **Record the event as described by the service member or witness.**
Use open-ended questions to get as much detail as possible.

_____
_____
_____
_____

Key questions:
- Can you tell me what you remember?
- What happened?
- Who were you last with?

B. **Observable Signs**
At the time of injury were any of these observable signs witnessed?
Visual clues that suggest a possible concussion include:

- Lying motionless on the ground
- Slow to get up after a direct or indirect blow to the head
- Disorientation, confusion, or an inability to respond appropriately to questions
- Blank or vacant look
- Balance difficulties, stumbling, or slow labored movements
- Facial injury after head trauma
- Negative for all observable signs

C. **Record the type of event.**
Check all that apply:

☐ Blunt object ☐ Sports injury ☐ Gunshot wound
☐ Fall ☐ Assault ☐ Explosion/blast Estimated distance ____
☐ Fragment ☐ Motor vehicle crash ☐ Other _____

D. **Was there a blow or jolt to the head?**

- Did your head hit any objects?
- Did any objects strike your head?
- Did you feel a blast wave? (A blast wave that is felt striking the body or head is considered a blow to the head.)
- Did you have a head acceleration or deceleration?

☐ YES ☐ NO ☐ UNKNOWN

Revised 10/2018 dvbic.dcoe.mil Page 2 of 14

Figure 1-3: MACE-2 Assessment Tool [8]

past TBI diagnostic tools have primarily focused on detecting neurological damage but recent research has suggested alterations to the glial cells and cerebrovasculature may also impact the full functionality of the brain [10]. For the case of these Soldiers and Marines, traditional imaging detection techniques could not detect the microtears resulting from the pressure strains due to discharged weapon noise.

Recently, the U.S. Navy and Marine Corps has embraced the concept of Distributed Maritime Operations (DMO), where components of the force are geographically spaced in a effort to assert Sea Control over a larger domain, introducing a significant challenge in providing medical support to all dispersed assets [3], [11]. As of 2023, the U.S. Navy had only two dedicated hospital ships. Although larger surface combatants and amphibious ships (Aircraft Carriers and Amphibious Assault Ships such as LHDs and LHAs) have substantial medical spaces and personnel onboard, the ratio of available beds and medical specialists to the total number of Sailors onboard these ships is still undermatched [12]. In contrast, most medium sized surface combatants with crews of less than 300 people, have only one dedicated medical specialist (an Independent Duty Corpsman or IDC) and no x-rays or significant lab testing abilities [3]. The U.S. Navy has acknowledged these shortcomings, and in 2023, announced funding was approved for the construction of three Expeditionary Medical Ships (EMS) each equipped with 4 operating rooms and 124 beds (shown in Figure 1-4) [13].

Figure 1-4: Rendered Illustration of the U.S. Navy's Expeditionary Medical Ships (EMS) [13]

Additionally, the new Spearhead-class expeditionary fast transport (EPF) starting with the EPF-14 will be built with greater health service capabilities [14]. Nonetheless, this is still a limited number of dedicated expeditionary hospital ship assets to be added to the fleet. Another tool that could help alleviate the shortage of available beds and medical physicians is improved onboard shipboard diagnostic tools. A more accurate diagnosis of injury would ensure smarter usage of limited resources available on a Sailor's own ship as well as quicker evaluation for the need for transportation to the finite number of better-outfitted assets.

Beyond diagnostic tools, understanding how the brain and other soft tissues deform under extreme loading conditions has applications to designing improved Personal Protection Equipment (PPE) which is often the first line of defense against traumatic injuries. Such research would provide the necessary insight to engineers who design helmets and other protective body gear for military members. For example, this gear could be built to better absorb the energy imparted from forceful blows but also to detect and alert others when significant injuries have occurred in order to prioritize transferring that person to area where medical attention can be prescribed.

1.1.2 Use of Mechanics for Disease Classification and Diagnostics

In contrast to a more objective based diagnostics approach, modern medical disease diagnostic techniques still heavily rely on observed measured physical quantities such as the speed or pressure at which fluids are transported around the body and the visualization of tissues (as in a x-ray or observing cells at a microscopic level). Typically, physicians will collaboratively make clinical diagnoses based on these qualitative patterns of observed physical quantities while reviewing the past history of the patient [15]. For example, for a cancer diagnosis, one of the first indications for the presence

of cancerous tissue is a physical lump that can be externally palpated. Next, an ultrasound may be utilized to study the exact tissue location and shape and how it is progressively growing. A fine needle biospy will allow the physician to study the tissue at a cellular composition level. Each of one of these metrics, physical palpation, measurements of the tumor's relative dimensions, and cell structure observations, are examples within a portfolio of information which is used by doctors to recognize patterns leading to a diagnosis. However, it is known that significant bias exists utilizing these current, more qualitative metrics, especially radiology, which is often the first step in the diagnostic timeline [16],[17]. The consequences of an inaccurate diagnostic test can be significant; resulting in possible over or undertreatment and increased insurance costs [18].

With the advancement of tools collecting more mechanics based bodily metrics regarding a tissue's state, and development of Machine Learning (ML) to sort through a plethora of existing biomedical data, it is hoped that traditional diagnosis procedures can be complimented by new types of data to transform the current diagnostic workflow into a more objective and reliable process. The development of diagnostic tools based on measuring mechanical metrics draws from the many studies that now show the vital role of mechanics in evaluating the functional state of various body systems such as the nervous [19],[20] and digestive systems [21]. For example, Halder et al. [22] utilized fluid mechanics principles along with ML to explain the physics behind numerous esophageal diseases. Creating their own parameter space called the VDL (virtual disease landscape), they were able to map measured physical quantities corresponding to the function state of the organ onto an existing landscape of known diseases. Not only could they distinguish known existing disorders using this technique but they were also indications that this tool could also be utilized to predict how the disease would progress.

The proliferation of cancer, in particular, is highly dependent on the competing biological and physical forces within, and surrounding, the cellular structure. Understanding these links opens pathways for new diagnostic methods and treatment strategies. Four physical cancer traits that are suggested to explain the biomechanical abnormalities in tumors are (i) elevated solid stress, (ii) elevated interstitial fluid pressure, (iii) increased stiffness and altered material properties, and (iv) altered tissue microarchitecture (see Figure 1-5). Of specific interest to this research, is the role of stiffness in evaluating the presence and severity of cancer.

Matrix stiffening occurs due to increased deposition and cross-linking of the Extracellular Matrix (ECM) or network of macromolecules and minerials that provide structural and biochemical support to surrounding cells [24]. Strain-stiffening behavior resulting from the application of mechanical stresses can also increase the stiffness of a matrix [23]. This increased stiffness in tissues can lead to activated signaling pathways which promote the tumor's growth. Studies in various cancer types including breast [25], liver [26] and prostates [27] have demonstrated that malignant tumors are stiffer than benign ones. These differences in stiffness are often detected by traditional physical palpation practices, so it is already an observed, albeit, qualitative piece of data, utilized by doctors to distinguish between healthy versus non-healthy tissues. However, the perception of differences in material stiffness when distinguished by

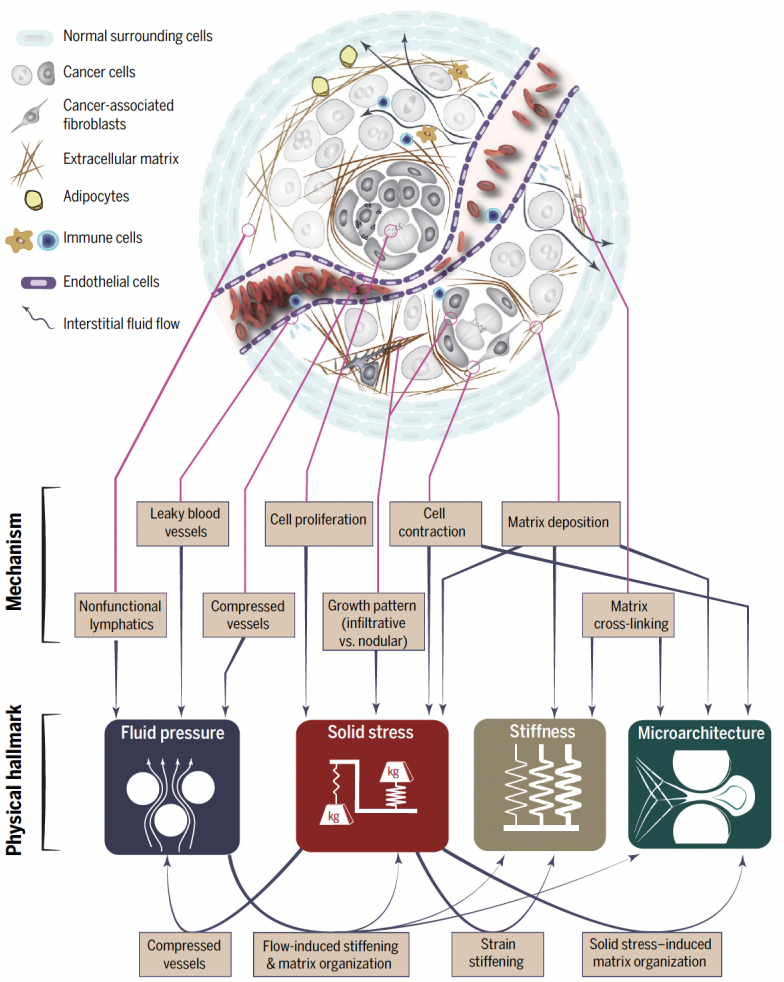

Figure 1-5: Origins of the Physical Traits of Cancer [23]

human touch is subjective to the person conducting the examination. Methodologies to collect quantitative, in-vivo stiffness data would help reduce these subjective distinctions.

1.1.3 Existing Methodologies for Determining Soft Material Mechanical Properties

Determining mechanical properties of biological tissues has important applications in creating more realistic biomimetric materials as well as improving disease detection and prognosis predictions [28]. However, there exist many challenges in determining these properties due to the complex hierarchical structure of biological materials. At each scale of interest, nano to millimeter level, the structure of a tissue can vary as well as the interaction of these hierarchical levels [29]. As a result of their inherent heterogeneity, these tissues also exhibit anisotropic and non-linear elastic behavior [30]. It is also vital to consider that removing a tissue from a body will impact the

measured mechanical properties since the surrounding structure imposes stresses that influence the tissue state. Additionally, over time, fluids in a tissue will evaporate and tissue will begin to degrade. Therefore, an tissue removed from the body will display different mechanical properties than the same tissue while it is still inside of an organism (in-vivo) [31], [32]. Lastly, due to their softer and more fragile nature, biological tissues are also more challenging to handle; often they cannot be easily affixed to traditional material testing devices without altering the state of the tissue. For all these reasons, capturing the full spectrum of mechanical responses of biological tissues has proven difficult.

In this next section, the specific shortcomings of many existing methods to capture mechanical properties of biological materials will be explained as they relate to the inherent complexities of tissues as previously described. The most traditional and well-known methods for testing material properties such as tensile, compression, and indentation testing (often used on solids such as metals and rubbers) fall short in their ability to test biological tissues because they often require altering the natural state of tissue once removed from the body to make the sample compatible with the existing test set-up. For example, in many blood clot studies, the clots must be injected into molds or cut or shaped in such a way to fit into existing holding mechanisms [33]–[35]. Other methods such as pulse wave velocity and pressure myography can only be utilized for specific applications such as studying blood vessel properties [28]. Additionally, methodologies such as elastography cannot determine characteristics of materials undergoing loading scenarios at both slow and very fast rates. Elastography also assumes linear elasticity, therefore the stiffness values calculated using this method can only be used for comparative purposes among the same tissue type [31], [36]. Lastly, many studies reviewing the existing methodologies as explained above, report orders of magnitude difference in material properties for a singular tissue such as blood clots [37] and liver [38].

Arguably, where existing methods for capturing mechanical behavior of biological tissues are most inadequate is in their ability to quantify mechanical properties under dynamic conditions. This application is extremely important for understanding what happens to a tissue when it is physically injured because this usually involves a tissue being subjected to an extreme loading scenario (fast loading rate). In the case of TBI's, especially, there is a notable lack of understanding regarding the strain and deformation mechanisms responsible for such injuries [39]. This can strongly be attributed to the shortage of mechanical characterization studies on human brain tissues relevant to modeling TBI scenarios. In their review, MacManus et al. [40] found only five existing studies where human brain tissue was exposed to strains and at strain rates that appropriately represent extreme loading conditions. This is due to the fact that replicating an "explosive" event in a safe and repeatable manner is challenging and the existing methods, as listed above, cannot measure and interpret the mechanical response of tissue during or right after such a disruptive event occurs.

Undoubtedly, there exists a need for a methodology that is more widely applicable across all biological materials that can yield both more accurate and consistent results. Furthermore, an ideal methodology will be able to probe tissues while they are still inside of an organism. It is also vital that this methodology is capable of capturing the

responses of tissues under extreme loading conditions, in order to capture the entire viscoelastic spectrum of behavior for biological materials, especially strain-stiffening responses.

1.2 Case Study: Thyroid Cancer Diagnostic Practices

1.2.1 Thyroid Cancer Background

Thyroid tissues consist of lobes enclosed in thin layers of connective tissues. The lobules produce thyroid hormones which regulate the body's metabolism and overall growth and development. The main anatomical components are shown in Figure 1-6.

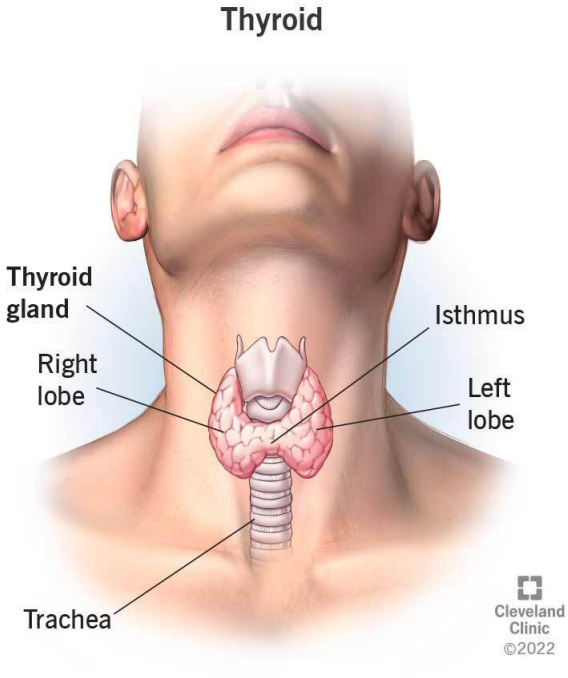

Figure 1-6: Anatomy of the Thryoid Gland and Trachea [41]

Thyroid cancer occurs less frequently, and has a relatively high survival rate, as compared to other cancers [42]. However, the development of nodules is relatively common, with a higher occurrence in women and persons of older age [43]. By age 60, 50% of the population will have a nodule discovered through imaging or during an examination [44]. Thyroid nodules are frequently, inadvertently, found during other routine medical procedures such as CTs or MRIs where the neck region is scanned. It is also possible for a patient or doctor to physically palpate that area and discover lumps which feel stiffer to the touch. Fortunately, only about 5-10 percent of nodules are cancerous [44]. However, due to the increasing availability of medical monitoring tools in the past few decades, it is suspected that over-diagnoses are significant [45]–[48].

After a nodule is discovered, a patient is typically recommended to see endocrinologist who will request an ultrasound. The Thyroid Imaging Reporting and Data System

(TI-RADS) is referenced for further classification of the suspicious nodule. If required, a Fine Needle Aspiration (FNA) (cellular level inspection) will be conducted, as shown in Figure 1-7. FNA involves the insertion of a needle into the targeted nodule in order to remove some cells. Once inserted, the needle must be aggressively moved around in order to dislodge enough cells for testing. This procedure can be painful to a patient especially if an inadequate amount of tissue is removed and the procedure must be repeated. Once an adequate amount of tissue is removed, it is sent to a cytology evaluation which is informed by the Bethesda Scale. As shown in Figure 1-8, this scale is used to communicate the ultimate diagnosis and recommended treatment [49]. A Level V or VI diagnosis primarily results in surgery. A Level III or IV diagnosis may result in surgery but typically it is attempted to clarify the diagnosis using other methods, such as molecular testing (molecular level inspection) before surgery is recommended.

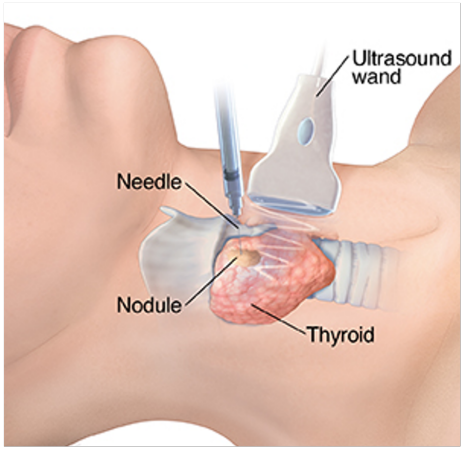

Figure 1-7: Fine Needle Aspiration (FNA) Procedure [50]

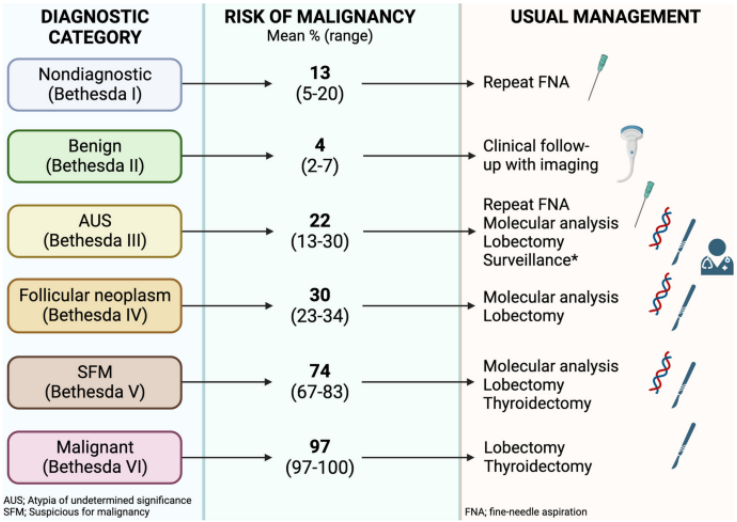

Figure 1-8: Bethesda Scale for Thyroid Cancer Diagnostics [50]

Through a combination of these diagnostic tools, approximately 5-7 percent of nodules are definitively marked as malignant. However, up to 40 percent of nodules fall under categories including indeterminate (15-30%), suspicious (3-5%), or non-diagnostic (5%) [49], [51]–[54]. A vast majority of the indeterminate category, if only classified through FNA, are reported to be benign on final surgical pathology (70-80%) [55]. This statistic can be improved (60-70%) with the use of molecular cytology but this test is more expensive because it is nominally conducted offsite from the hospital [55]. Figure 1-9 summarizes the efficiency of the current state of thyroid cancer diagnostics.

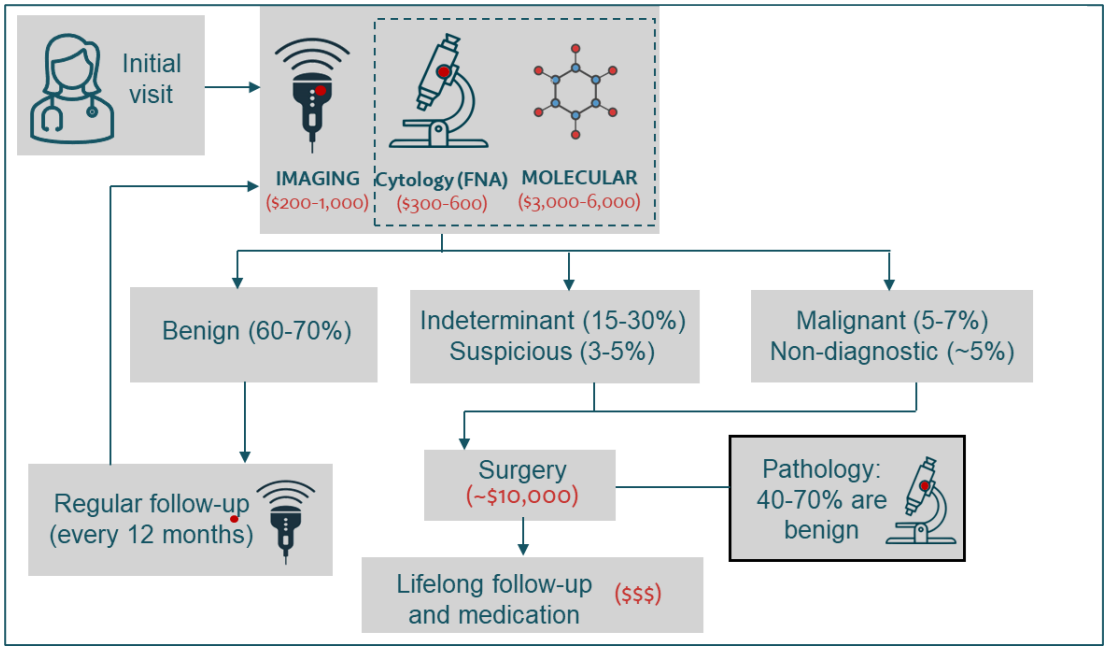

Figure 1-9: Existing Thyroid Cancer Diagnostics Flowchart

The negative impact of an unclear diagnosis could be a lobectomy or thyroidectoctomy. Once a portion of the thyroid is removed, the patient may be required to take thyroid hormone replacement therapy for their lifetime. Additionally, vocal cords, nearby nerves and other glands that control calcium levels are also at risk of damage during this type of surgery [56]. Due to the expense of current diagnostic tools and inconvenience and lifelong impact of such a surgery, there is room for improvement among the current thyroid cancer diagnostic tools.

Chapter 2

Experimental Developments and Techniques and Research Objectives

In this section, the origins of the VCCE methodology will be explained as well as summarizing past results of using this testing method on synthetic, and a few biological, material samples. This will be followed by a brief overview of VCCE procedure, specifically focusing on the key steps and corresponding pressure profile features that result in achieving a successful test. The identification of these features are proposed important pieces of information that may be used to identify a specific tissue. Additionally, this section will discuss the device setup used to perform the VCCE methodology in all past experiments as well as the current version of a portable device more suitable for eventual in-vivo applications. In conclusion, the research objectives of this thesis will be presented.

2.1 Historical Development of VCCE Methodology

The VCCE methodology was developed to facilitate instantaneous stiffness measurements [57], [58]. This methodology involves injecting a known volume of incompressible fluid into a material cavity (see Figure 2-1). A pressure sensor, connected to the injection needle, monitors the cavity pressure during both active expansion of the cavity as well as passive relaxation once no more liquid is being injected.

The VCCE technique is derived from a methodology known as Cavitation Rheology (CR) [59], [60]. The first iteration of CR similarly employed a needle probing technique but utilized compressed air. Initially, in this method, the pressure of injected air was steadily increased over time resulting in relatively small changes of cavity volume until a mechanical instability limit was reached and the volume changed significantly, instantaneously. The desired result of these experiments was to measure a “critical pressure" at the onset of mechanical instability [59], [60]. However, it was noted in subsequent experiments that the sample often fractured before the cavitation instability limit was reached [57]. Furthermore, the use of this critical pressure value to calculate a equivalent modulus also relied on the assumption of the neo-hookean strain-energy model which is not a valid model when inflicting large strains on strain-stiffening

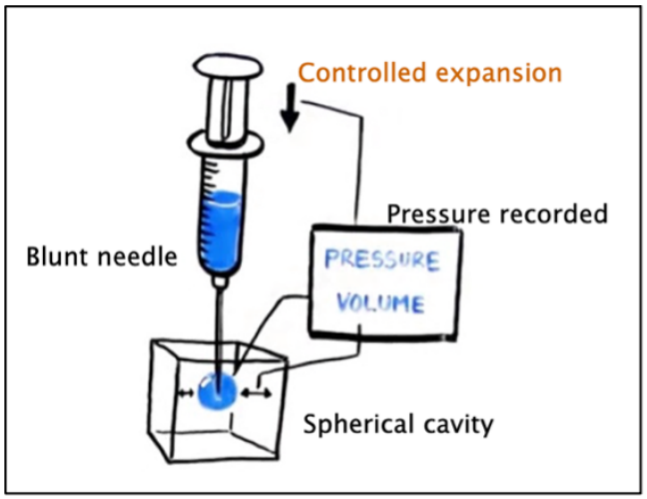

Figure 2-1: Block Diagram Description of VCCE Methodology

materials such as biological tissues [61]. Raayai-Ardakani et al. [57] modified this protocol by employing an incompressible fluid, instead of air, and attempted to control the volume of the system instead of the pressure. This methodology was perfected through the development of the VCCE. By controlling the volume, VCCE obtains not only a peak pressure (i.e. a single value of interest) but an entire nonlinear volume-pressure curve, similar to an equation of state. This method can also track the mechanical response beyond the critical pressure, to obtain and elucidate the fracture properties.

Raayai et al. [57] initially demonstrated the VCCE technique with Polydimethylsiloxane (PDMS) samples of varying base:cross-linking agent ratios (33:1, 37:1, 40:1, 42:1, 44:1, and 50:1), focusing on determining elastic material properties. In these experiments, a Constant Volume Expansion (CVE) methodology was utilized. However, Chockalingham et al. [58] improved upon this technique to fully capture the viscoelastic range of behavior of PDMS by implementing a version of the VCCE procedure that expanded the volume of the fluid cavity at a constant radial rate (or Constant Radial Expansion (CRE)). Therein it was shown that keeping the stretch rate constant during expansion was key to capturing both the quasi-static and dynamic material parameters of soft materials such as biological tissues.

There is also precedent for the conduction of the VCCE methodology in biological tissues. Mijailovic et al. [61] used VCCE to calculate the Young's modului for porcine and murine brain sections. Varner et al. [37] tested a range of constant radial expansion rates on bovine blood clots and was able to observe stiffening behavior as well as the softening of clots as they aged. In all of these initial experiments with both the synthetic and limited biological tissues samples, it was possible to implement complex rate profiles to determine mechanical properties of materials due to the specific laboratory testing device and supporting equipment utilized. However, replicating such profiles outside of a lab setting was not yet proven possible and it was not clear how this could affect potential diagnostic applications.

2.2 VCCE Pressure Profile Description

In each of the following subsection descriptions, the purpose of key steps in the VCCE methodology will be presented, followed by a discussion of the expected results of these steps as established by the historical precedent of testing in a synthetic, biomimetic material known as PDMS. Lastly, the differences in testing of a synthetic versus biological material will be identified as well as hypothesized alterations to the existing VCCE protocol to obtain similar anticipated outcomes as observed while testing in synthetic materials.

Needle Insertion and Retraction

Experimental procedure: During this prerequisite step before fluid injection, an initial defect is created in the material. An initial defect is created because if the needle was inserted without retraction, the compressed material beyond the tip of the needle would form a plug that blocks the needle opening [62]. To make this initial defect, a needle is slowly inserted until the surface of the material is ruptured. This step of the insertion process can be monitored both visually and by observing the pressure readout.

Earlier results in PDMS: As initially demonstrated in PDMS (see Figure 2-2), the pressure was observed to monotonically increase until the material surface was broken [62]. Next, the pressure would sharply drop in the immediate moments after rupture before slowly decaying towards a zero pressure or relaxed state. However to accelerate this decaying process, the needle could be retracted slightly (a few millimeters) resulting in a small defect.

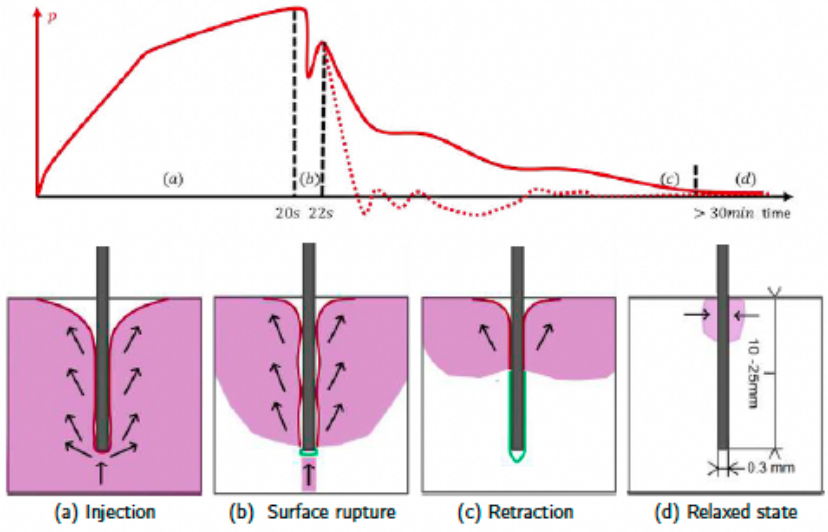

Figure 3.8: Pressure evolution during needle injection and corresponding injection steps, as the needle is actively retracted (dotted) or left in place to relax (solid). Material withstands large deformation without permanent damage (a) before surface rupture (b) allowing the material to gradually relax residual stresses. The process is accelerated by retraction of the needle (c) shortly after ruptured. After relaxation time (1-4h) residual stresses are mostly dissipated except for radial stresses (d).

Figure 2-2: Pressure Profile During Insertion and Retraction [62]

Expected biological challenges: For a particular PDMS sample, very consistent insertion and retraction distances could be established resulting in nearly ideal pressure profiles during this step. However, these distances were altered when VCCE was performed in blood clots, for example, because the surface was easier to rupture [37]. It was predicted that for more heterogeneous biological tissues, the retraction and insertion distances may vary more greatly between tests and that pressure profiles will be less consistent (e.g. different peak pressure when the surface is ruptured and/or varying pressure gradients to reach the peak pressure).

Injection Phase

Experimental procedure: The purpose of the injection phase is to fill the fluid cavity with an incompressible fluid which stretches the material encompassing the cavity until fracture occurs. This fracture is a result of energy release, associated with the cavity expansion, into the surrounding material. As shown in Figure 2-3, upon initiation of fluid injection, the corresponding pressure will initially exponentially increase. This is also known as the elastic expansion phase. The critical pressure of when fracture initiates is another potential valuable piece of information from the injection phase. After initial fracture, the pressure will remain non-zero because more fluid is still be injected into the material.

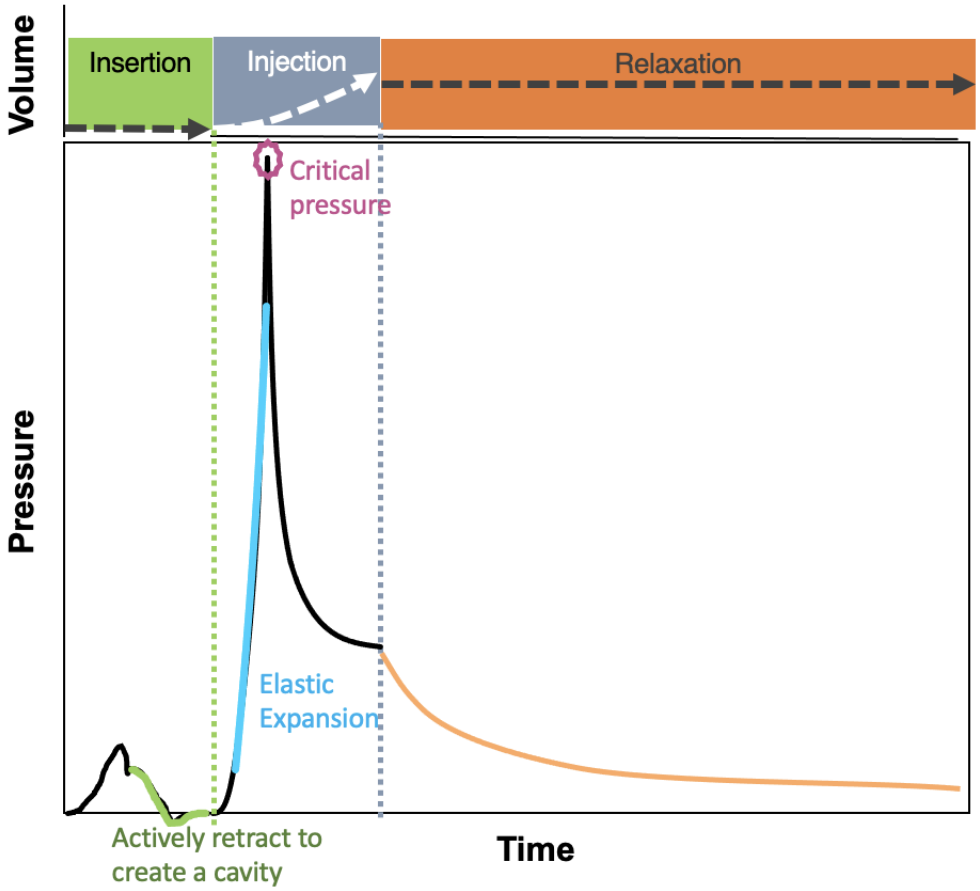

Figure 2-3: Key Features of Pressure Measurements during VCCE Test Sequence

Earlier results in PDMS: For synthetic materials such as PDMS, existing material models such as the neo-hookean model has been effectively fitted to parts of the elastic expansion slope to calculate a reasonable corresponding stiffness value [58]. Importantly, during this expansion process, it is assumed that the fluid cavity is expanded nearly spherically so one can estimate the approximate effective radius. The effective radius during elastic expansion is a key piece of information required for the material model fitting process. Of note, it was previously shown in PDMS, that expansion may originate from defect that is non-spherical but any error introduced by this initial non-spherical cavity is negligible during the expansion process [57], [61]. For testing in PDMS, this nearly spherically expansion could be visually observed. In regards to the critical pressure at fracture for PDMS, at certain base:cross-linker ratios, this value has been shown to remain relatively similar between tests.

A common, inadvertent result during the injection phase is when fluid leaks from the cavity before initial fracture occurs, this is often to due to a poor seal between the needle opening and defect. In PDMS, this can be observed visually just as the fluid begins leaking up the needle (Figure 2-4). Fluid leaks in PDMS will still appear on the pressure profile during injection as successful expansion tests, however, the anticipated behavior after fracture will look different. An example of this occurring is shown in Figure 2-5. On the left most plot, one observes the pressure to slowly decrease once injection ends but on the right plot, the pressure is shown to suddenly flatten and stays relatively constant once the leak began.

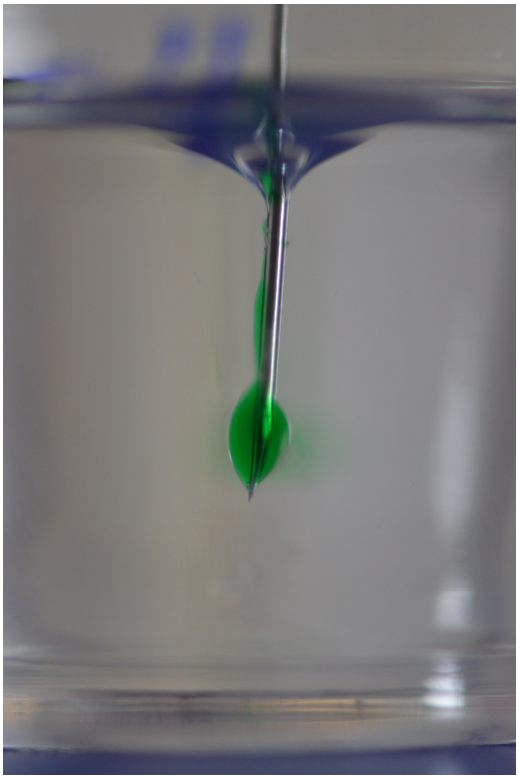

Figure 2-4: Leaking of Fluid up the Needle during VCCE Test in PDMS

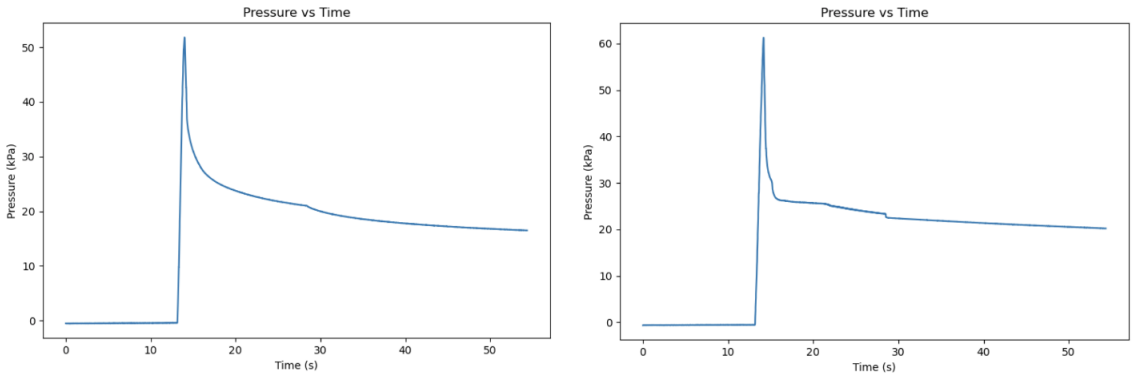

Figure 2-5: Observation of Leaking in Pressure Profile for PDMS

Expected biological challenges: It is known that the visual observation of the cavity expansion process will not possible in tests on biological tissues, however instances of leaking will still be visible because fluid will flood from the opening of the needle insertion site before the injection stage has completed.

Material Relaxation Phase After the injection phase stops, the material will begin the process of relaxation. This is an important component of pressure profile because as shown in Figure 2-3, the pressure does not immediately decrease to zero. This thesis will not focus on the characterization of this portion of the pressure curve.

2.3 Instron Setup and Experimental Procedure

The VCCE procedure was initially enabled through the use of an Instron Electropuls 3000 (Norwood, MA, USA) controlling the plunging of a 50µL syringe (Hamilton GASTIGHT of Reno, NV, USA) filled with fluid into a sample of interest (Figure 2-6). The pressure experienced during fluid cavity expansion was measured by a PRESS-S-000 luer lock connected pressure sensor (PendoTech, Princeton, NJ, USA). Using a pre-made constant volume or constant radial expansion profiles created in WaveMatrix, the precise injection of fluid into the sample was controlled. A real-time readout of the pressure can be observed during the fluid cavity expansion using this program (as well as the history of pressure during the course of test). Although the Instron device and supporting components have been effective in capturing the desired pressure data as previously discussed, there were many challenges observed with utilizing this setup specifically regarding future in-vivo tissue application. These challenges such as the syringe re-fill procedure, control of the sample height during the insertion and retraction step, and the protocol for taking and organizing notes related to each individual test are discussed in subsequent paragraphs.

One of the first steps before beginning a VCCE test is to fill the syringe assembly with a testing fluid. To remove the syringe assembly, numerous nuts and blots holding the fixed support plate must be detached. Care must be taken to replace these components precisely and under equal tension. Additionally, the placement of plate assembly must be aligned directly centerline to avoid generating a static friction force

Figure 2-6: Nominal Instron Setup for VCCE Lab Experiments

which can impose bending on the fixed support plate holding the syringe resulting in a “mechanical compliance" error [62]. This process is time intensive and air entrapment during needle installation, and after prolonged testing periods, is a common problem. Furthermore, even if a visual air bubble is not observed when replacing the syringe assembly, a calibration test must be performed once the syringe assembly is fully reinstalled to ensure compliance due to air entrapment is negligible. If the results of this calibration test show “non-mechanical compliance", the process of replacing the needle tip and more carefully removing any entrapped air from the syringe assembly must be performed again.

When performing either a calibration or a singular expansion test, a container of either the testing fluid or sample of interest is placed on an adjustable, cross-hatch staging mount. This stand is manually adjusted by experimenter during the insertion and retraction process to ensure the optimum cavity size is created and to monitor pressure during this process. The number of knob turns correspond to a certain vertical distance that the needle is being plunged into and out of the sample and can be calculated using simple geometry.

The Instron testing device and Wave Matrix tool do not inherently incorporate the ability to record observations about the environmental conditions surrounding each test (temperature and humidity of the lab, the purpose of performing each test etc.) simultaneously as the tests are being formed. Instead, the user performing the VCCE test must manually record notes in the application of their choice, later compiling and correlating these notes to each test.

2.4 General Purpose Research Tool (GPRT) Description

The General Purpose Research Tool (GPRT) is a portable, dedicated VCCE testing tool version of the Instron setup, developed by fellow lab member Brendan Unikewicz. The testing protocols were developed in Python and run through the Virtual Studio (VS) Code interface. The desired application of this tool is enabling the use of VCCE to determine quantitative material properties of soft tissues. Adapting the VCCE traditional methodology into a portable tool form, with minimal training required to easily operate it, is a step towards preparing this procedure for eventual use in a clinic setting [63]. The main components of the GPRT are shown in Figure 2-7.

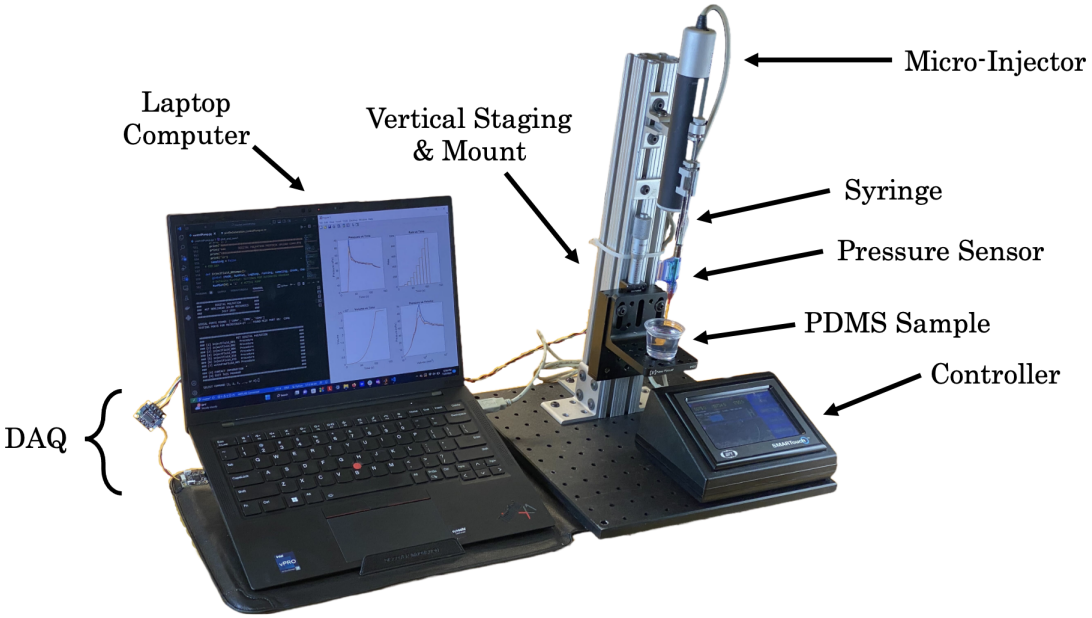

Figure 2-7: Labeled Components of the GPRT [63]

2.4.1 GPRT Testing Procedure

This tool utilizes a micro injector device to dispense controlled amounts of testing fluid into the sample. The pressure sensor is the same type utilized in the Instron setup but is connected to the DAQ (data acquisition system) which converts the analog, electronic signals produced by the pressure sensor into digital signals through the use of an ADC (connected through a USB) to the computer. The controller device

communicates commands from the computer to the micro-pump injection device. It can also be operated manually to reset the syringe position (refill) before the beginning of each test. The vertical staging component of the device incorporates a micrometer which can easily be read to monitor the insertion and retraction distances into the test sample. Other key specifications of the GPRT are listed below:

- Weight: ∼15 lbs
- Dimensions: 18”(L) x 18”(W) x 25”(H)
- Power: 100-120V
- Needles: Disposable, 25G, 1” length, Luer lock (Blunt and Beveled typical)

The following section provides a general timeline and brief description of each step when conducting a VCCE test on a tissue sample using the GPRT:

Steps Performed **without** Tissue Sample (**Total Time: 5-10 minutes)**:

1. An initial calibration test must be performed for each type of test or whenever a needle is replaced. This test is performed in a Phosphate-buffered Saline (PBS) solution and must be reviewed directly after test completion to ensure proper function of the device **[3 minutes]**.
2. Prior to beginning each new test within a sample, all fluid is purged from the syringe and pressure sensor and then flushed with a bleach solution (if testing any type of biological tissue) **[2 minutes]**.
3. If needle replacement is necessary (testing a normal portion of sample versus a diseased portion or testing an entirely new tissue sample), entire syringe assembly must be flushed **[5 minutes]**.

Steps Performed **with** Tissue Sample **(Total Time for Singular Test: 10-15 minutes)**:

1. For each test within a specimen, the needle is inserted and retracted a set distance via a mechanical stage. Pressure is closely monitored during this process and this "Insertion Data" is recorded and reviewed immediately before beginning a test to note any unexpected or unusual behavior. Occasionally, a five minute holding period is warranted to allow the material to relax **[2-7 minutes]** (see Figure 2-8).
2. The computer and syringe pump control the creation of the small cavity at a prescribed rate **[3 minutes]**.
3. Results reviewed in real time **[2 minutes]**.
4. System is re-set for second probing (replace needle if necessary, clear syringe, and refill) **[2 minutes]**.

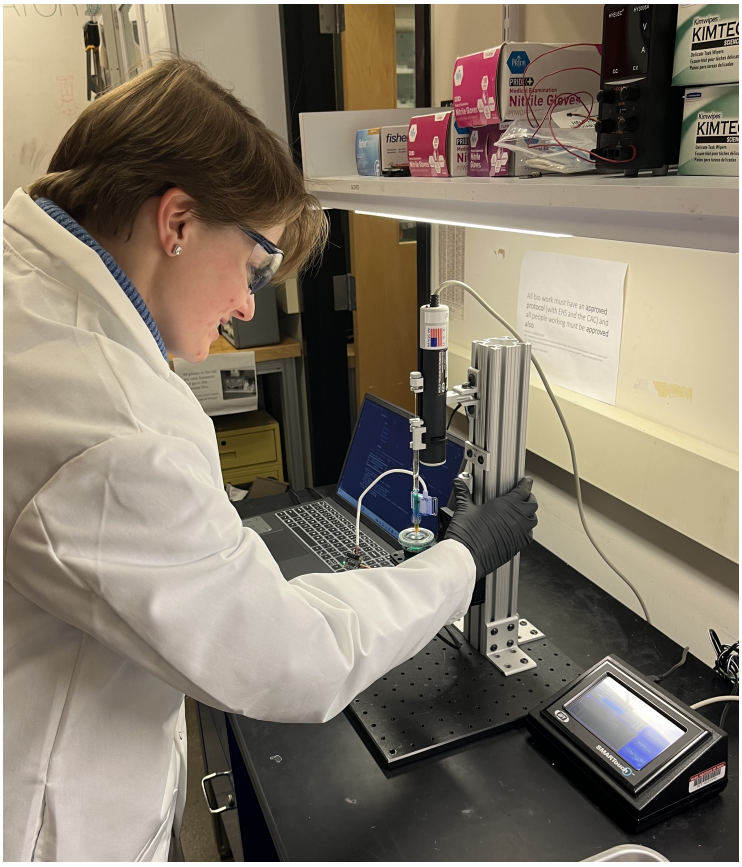

Figure 2-8: Laboratory Device Setup

2.5 Instron vs. GPRT: Differences in Device Setups

There are numerous differences between the Instron and GPRT device setup. The following section describes how these differences impacted the types of tests that could be conducted on the GPRT as well as the quality of data that was produced by this device.

Unikewicz et al. [63] noted that the rotation of ball bearings within the micro-injector motor transmitted a significant pulsating force to the syringe assembly which was subsequently felt by the pressure sensor. To ensure this force was negligible as compared to the inertial force of the fluid cavity as it expands, a syringe with a smaller cross-sectional area than that utilized for the Instron device was selected (10μL). Due to utilizing the 10μL on the GPRT, the largest maximum radius of the fluid cavity that could be achieved was $\approx 1.3mm$. However, this radius is well beyond the size of cavity which would induce fracture. Additionally, the anticipated elastic portion of interest during fluid cavity expansion is nominally experienced in the first 0.2 to 0.5mm of radial expansion.

Past VCCE experiments on the Instron have utilized various combinations of syringe and needle sizes based on the limitation of tools used at the time to perform the procedure. Especially in the development phase of only being able to perform CVE

expansion tests on the Instron, it was critical that the achievable cavity sizes were consistent with the length and cross-sectional area of the syringe to ensure constant stretch rates were achievable during a portion of the initial cavity expansion. This was vital in ensuring the full viscoelastic behavior of a soft material was captured. Thereafter, it was demonstrated that using a larger syringe size resulted in less certainty regarding the accuracy of the effective cavity radius [62] so while initial testing was performed with a 3mL syringe on the Instron device [57], it was proven to be more desirable to utilize a smaller size (50µL) syringe for follow-on experiments. Subsequently, the selection of 10μL for the GPRT falls well within the desired syringe size.

The GPRT was restricted to conducting CVE tests due to the controller's low storage memory [63]. The syringe micro-pump injector was also optimized for discrete control (utilizing a singular expansion rate). Although, Unikewicz et al. [63] note that "pseudo-continuous" control is possible, the controller lags in executing this new command resulting in a delay to the real-time change in cavity expansion rate. As previously mentioned, during a CVE test, the radius of fluid cavity changes during the course of the procedure so the stretch rate is *not* constant. As illustrated by Raayai-Ardakani et al. [57], experiments with constant volumetric rate expansion resulted in large stretch rate variations (typically very fast at first and then slowing to a more constant rate as the cavity size reaches 1.2mm) that led to a saturated material response inadequate for the full characterization of viscoelastic materials [58]. However, for certain applications, such as diagnostics of disease, it is suggested that it may be adequate to only characterize the instantaneous material response i.e. minimize compliance by assuming one spring constant goes to infinity.

The micropump selected for the GPRT was also limited in the injection rate it could dispense. The maximum injection rate for the 10uL syringe is 657μLps [64]. Due to the motor-thread engagement distance, some volume of 10,000nL syringe also cannot be utilized ($\sim 80\mu$L). Assuming a 1.3 millimeter maximum cavity radius, and knowing the amount of available fluid in the syringe, a 600μL CVE test was selected for the majority of tests conducted on biological tissues. The 600μLps test takes approximately 15 seconds to conduct with a 10μL syringe. Reducing the total testing time was important for the application of this device in a hospital setting. With this injection rate maximized, this current iteration of the GPRT was ill-suited for capturing high loading rate material responses but as previously stated, for the specific application of cancer diagnostics, this limitation did not affect the device's ability to capture the instantaneous stiffness behavior of the biological tissues tested.

The process of refilling the syringe assembly was greatly simplified with the GPRT setup because the time to remove and replace the syringe assembly from the device was significantly reduced. To remove the syringe assembly, one must simply loosen the top screw that holds down the syringe and pinch the sides of the holding device around the syringe body (Figure 2-9a). To replace, the same steps are performed inversely. Another improvement of the GPRT was the inclusion of a micrometer which allows the experimenter to directly read off insertion and retraction distances during the cavity creation process (Figure 2-9b).

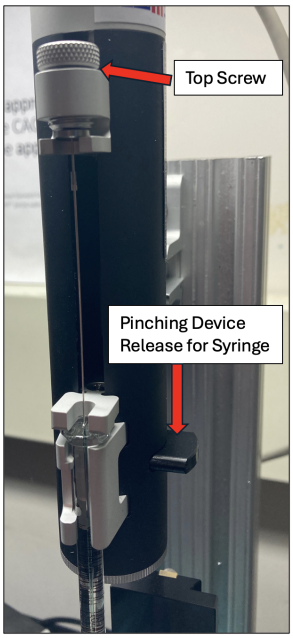

(a) Syringe Assembly Control Points on GPRT

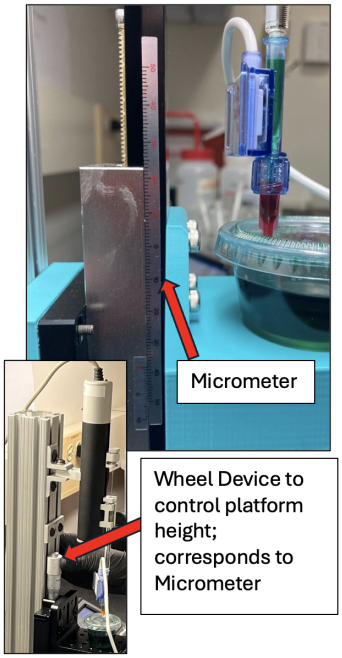

(b) GPRT Micrometer

Figure 2-9: GPRT Syringe Assembly Control Points and Micrometer

The GPRT also enhanced the user's experience of taking notes related to the environmental conditions and other observations during the course of a test by including a series of prompts in the program, such as humidity or cross-base ratio for PDMS samples. After the completion of each individual test, these notes were automatically compiled into an csv file for easier, future data analysis.

2.6 Research Objectives

The purpose of this thesis is to discuss some of the implementation challenges for utilizing VCCE as an in-vivo, biological tissue, bulk mechanical property testing methodology.

- **Investigate needle choice.** Prior VCCE testing in both ex-vivo brain tissue and blood clots utilized a blunt tip needle. For eventual application to in-vivo tissue testing, a needle with a bevel would be required to minimize injury to the patient and to penetrate the outer skin layers in order to probe internal organs. Therefore, VCCE tests were conducted in synthetic and biological tissues with a beveled needle to determine if this needle type would affect the ability to achieve the anticipated pressure profile using the traditional VCCE methodology. Furthermore, the needle length and gauge was altered in various tests to determine if a particular needle is best utilized for certain tissue applications.

- **Investigate transition to miniaturized VCCE test set-up.** The VCCE methodology was initially performed utilizing the Instron testing device, however, this instrument is not portable, is expensive, and requires extensive training to operate. The GPRT was developed as an alternative tool to the Instron that can perform the VCCE method outside of the traditional research laboratory setting. To evaluate the effectiveness of this tool, initial testing was conducted in synthetic material substitutes and biological tissues to determine if the key features of the traditional pressure profile were achievable. Limitations were noted for suggested design changes that would be required for the use of this tool in eventual in-vivo applications.

- **Application of VCCE in thyroid tissue.** Another desired application of VCCE is for tissue diagnostics, whether this is to diagnose damage from a blunt force injury or cancerous cell growth. In collaboration with Newton-Wellesley Hospital, the GPRT was taken into a hospital setting and used to probe extracted human thyroid tissues. The many difficulties of working with diseased tissues were noted for future improvements to the GPRT and the overall testing methodology.

Chapter 3

Refinement of VCCE Technique for Various Material Testing

This section will begin by explaining the reasoning behind selecting a certain needle type for performing experiments in all prior VCCE work. This will motivate the initial experimentation comparing various needle types in PDMS and bovine blood clots, with a particular focus on understanding if a beveled needle could be used to perform the VCCE methodology for eventual in-vivo tissue applications. The results of these tests informed the transition of testing new biological materials such as bovine liver and swine thyroid using the GPRT. These experiments demonstrated that specific needle types and steps of the predefined VCCE protocol may require alterations in order to successfully conduct VCCE in different biological materials.

3.1 Background on Needle Characteristics

The bevel angle, gauge size, and length are three crucial needle characteristics to alter depending on the desired application. For most needle applications, bevel type is typically broken into three sub groups to include regular, short, and intradermal. However, there are far more specialized applications for needles that may involve utilizing multiple bevel angles in a singular needle tip. A needle used for a certain application is normally described by the bevel type [65]. The corresponding gauge range and bevel angle can still vary within that bevel type group. A regular bevel needle is nominally cut at 12 to 15 degrees and is most commonly utilized for intramuscular and subcutaneous injections. The sharper angle ensures the needle will less painfully puncture through skin layers to reach deep muscular tissue. The short and intradermal bevel angled needles tend to have shallower bevel angles and are typically applied at a less steep angle to the skin for applications such as IV injections and nerve blocks. A 90 degree bevel or blunt tip needle is typically used in non-medical applications because this penetration shape will cause the greatest damage to surrounding tissues during penetration [66].

The gauge size describes the hollowness of the needle (for example, 23G needle = 0.02525 inch or 0.6414 mm (outer diameter) - 0.01325 inch or 0.337 mm (inner

diameter)). A larger gauge number corresponds to a smaller diameter needle. Smaller diameter needles are less painful to insert and reduce tissue damage because they minimize the amount of total force (or injection force) imparted [67]. The tradeoff is a thinner needle tends to deflect more upon insertion. The length of needle impacts what tissues can be accessed. A longer needle may theoretically be able to penetrate deeper tissues but it can be more vulnerable to bending stresses.

3.2 Precedent for VCCE Needle Selection

Past VCCE testing has solely utilized a 25G or 22G, 1 inch needle to test materials such as PDMS, blood clots and brain tissue [37], [57], [58], [61]. These needle gauge sizes are considered mid-sized within the available range of gauge sizes. One study, specifically involving the testing of brain tissue [61], utilized a 22G needle to minimize surface tension effects. A length of 1 inch was selected to ensure there was an adequate amount of needle length required to break the surface of the material without the Instron's upper syringe assembly interference. Additionally, most samples tested using the Instron device setup were placed in a 1 ounce or 30mL plastic cup where a 1 inch length needle is ideally suited for penetrating nearly half-way down the cup height while ensuring the cavity is expanded far from any boundary.

Additionally, in all material tests, a blunt tip needle was utilized. With a blunt tip needle, it is easier to expand the fluid cavity beyond the needle tip, minimizing any interference of the needle itself on the cavity expansion. It has also been shown that even when the fluid cavity is not expanded perfectly spherically beyond this needle tip, the volume injected is still nearly spherical [57]. A blunt tip needle could also be utilized for testing in all prior experiments because all previous testing materials were generally softer with relatively heterogeneous internal structure, making these materials easily penetrable. Christine Roth [62] briefly discusses the choice of a blunt versus beveled needle when she conducted VCCE tests in nearly transparent PDMS samples, this was insightful because she able to observe the cavity expansion visually. If a needle with a bevel was utilized, Roth observed the fluid cavity migrating up the point forming a sphere surrounding the needle rather than right beyond the tip (Figure 3-1). However, she also noted better control of the cavity expansion process which has important implications for consistent testing results. In general, Roth [62] also observed that the penetration depth required to break the surface of material was smaller with a beveled needle so the relaxation time required for the material to not be strained by needle movement was shrunken. Although these observations may help predict the anticipated outcome of using a beveled needle in a biological material, as previously stated, PDMS is a much more homogeneous material.

Initially, testing in PDMS and bovine blood clots for this thesis began with using the same needle gauges as demonstrated in previous work (23G and 25G, 1" needles). However, for these experiments, both blunt and beveled versions on these needles were also utilized.

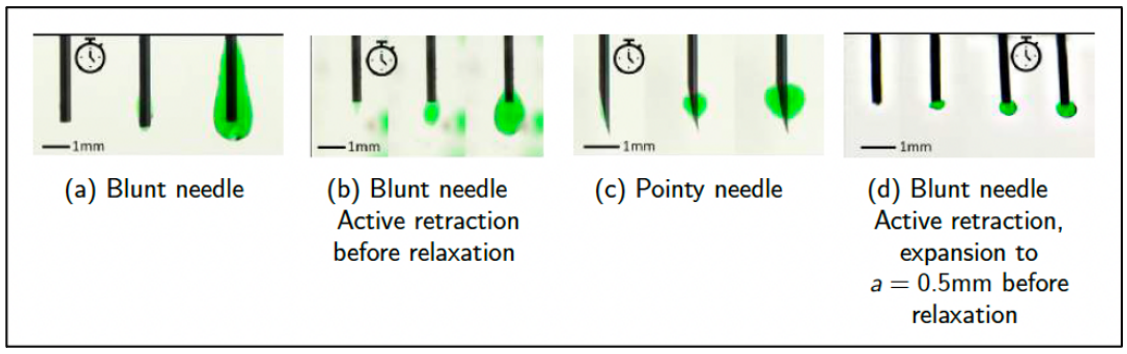

Figure 3-1: Photos of Fluid Expansion Cavities for Blunt vs. Beveled Needles in PDMS [62]

3.2.1 Needle Selection for Human Thyroid Cancer Diagnostic Testing

For human thyroid cancer diagnostic testing, many of the current tools also involve needle based probing techniques such as fine needle aspiration cytology (FNAC) and needle core biopsy (NCB). While the ultimate goal of both these procedures is to yield a small extracted piece of tissue for ex-vivo analysis, the selection of how this needle gauge size has affected the success of these methods was of interest to this research.

The success rate of FNAC and NCB is typically assessed based on how many attempts are required to extract enough useable sample for analysis while trying to minimize pain experienced by the patient. For FNA tests, needle gauge sizes between 21 and 27 are commonly utilized. One study found that while using 21G and 27G needles for FNA of human thyroids, there was no statistical significant difference in the cytopathological results of specimens obtained with both types of needles, although larger needle size tended to be associated with more complications [68]. Another study, that compared the use of 22 versus 25G needles for FNAC, concluded that the gauge size do not significantly impact the pain experienced by the patient. However, the number of times the procedure had to be performed significantly impacted the pain experienced by the patient. Another key finding was that, a larger diameter needle (22G) was able to penetrate calcified nodules more often than a needle of smaller diameter (25G) [69].

Another important distinction between how traditional human thyroid cancer diagnostic tests are conducted and the VCCE methodology, is the speed at which the needle is inserted into the desired testing tissue. For the FNA procedure, the needle is injected swiftly into the suspicious nodule (<1 second) and vigorously moved to and fro multiple times through the nodule in order to extract cells. For the needle insertion and retraction steps of the VCCE methodology, these steps are typically performed more slowly (≈10 seconds total) and there is minimal needle movement once the nodule or tissue location of interest is reached before retraction of the needle. This is in an attempt to reduce the amount of damage inflicted by the needle itself penetrating into the tissue structure. Some authors additionally propose the speed of insertion is connected to the insertion force into various tissues [70]. In their experiments, Jiang

et al. [66] demonstrated that different tissues (skin, muscle, fat, liver capsule and vessel) generate various force cures, which will also impact the most efficient insertion strategy to utilize on each type of biological tissue. Clearly, it will be vital to future refinements of the VCCE procedure to find the balance between applying the minimal force to penetrate a tissue while also inserting the needle as quickly as possible in order to minimize, internal tissue structure damage once an outer structure is breached and, pain imparted to the patient. For this reason, the VCCE needle insertion protocol as it is conducted in various biological tissues may need to be altered.

3.3 Needle Comparison Tests in PDMS and Bovine Blood Clots

Preliminary needle comparison experiments were conducted in PDMS and Bovine blood clots since it was known that minimal to no alterations to the nominal VCCE protocol were required to conduct successful tests in these materials. The purpose of these tests was to explore how needle length, diameter size and presence of bevel may have affected the anticipated pressure profile.

3.3.1 PDMS

PDMS is a commonly used synthetic substance that mimics the viscoelastic behavior of biological materials. It can be mixed at varying cross-linking agent ratios to change the time-dependent elastic behavior, so as to model a range of different soft materials. However, the internal structure of PDMS is notably more homogeneous than that a typical biological tissue. Per procedure as described in [58], 45:1 (base to cross-linker ratio) samples were mixed in plastic sample cups and allowed to cure for 2 hours in a oven at 100°C.

Using the original Instron set-up, both CRE (0.02mm/s and 0.32mm/s) and CVE tests (.402mm^3/s and 2.684mm^3/s) were performed in the 45:1 PDMS samples. These rates were selected because they have been successfully demonstrated to achieve elastic expansion in previous work [58], [62]. As similar pressure profile observations were made utilizing both CRE and CVE tests, the focus of this section will be on the CRE tests only. For these experiments, a blunt 25G 1", blunt 25G 5/8" and a beveled 23G 1" needles were utilized. As shown in Figure 3-2, it was possible to achieve the expected pressure profile using all three needle types. However, some observations about the defect size and subsequent achievable stretch rates as well cavity growth location relative to the needle opening are explained in subsequent paragraphs.

In general, it was observed that the initial defect created during the insertion and retraction steps was larger for a larger diameter needle and for a beveled versus blunt tipped needle. This is shown in Figure 3-3 (right plot). Intuitively, the larger diameter needle would create a larger initial defect but understanding why the beveled needle would create a larger defeat over the blunt needle had a more nuanced explanation. Although it was known that the shape of beveled needle would create nearly the same radial size cavity as it is plunged through the sample, in order to withdraw the needle

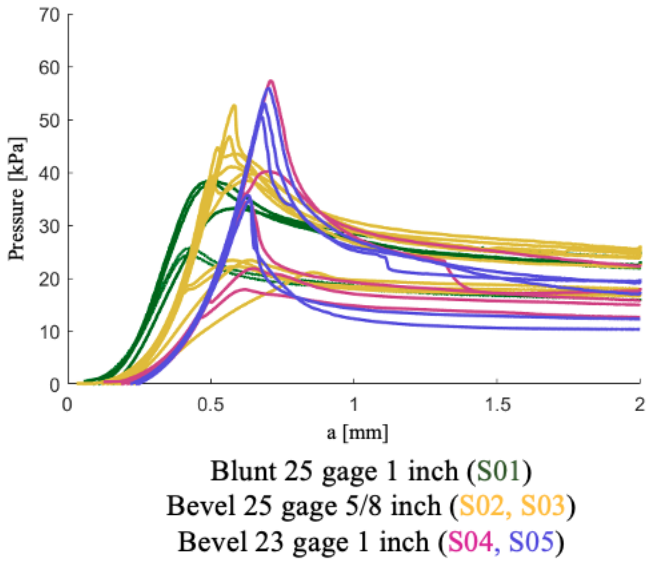

Figure 3-2: Constant Radial Tests in PDMS: Radius vs. Pressure

to a equivalent height of retraction, as shown in the left most illustration in Figure 3-3, the surface area impacted by the shape of the needle opening will be greater for the beveled versus blunt.

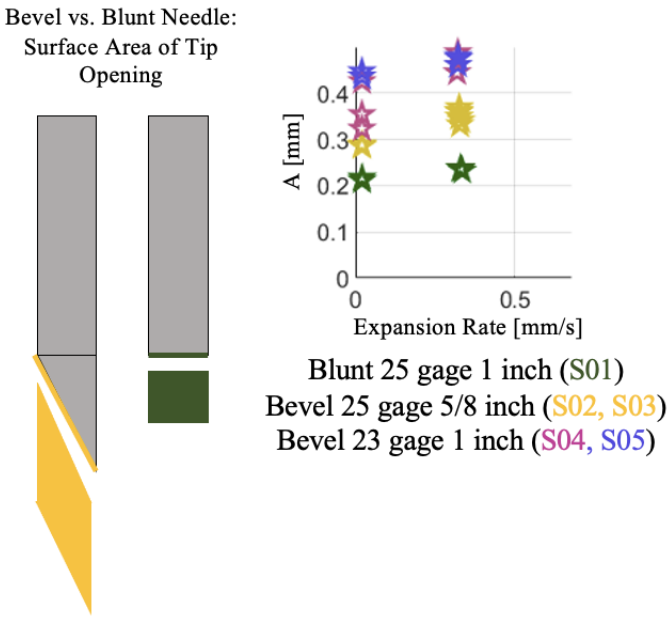

Figure 3-3: Needle Comparison Tests for Constant Radial Tests in PDMS: Expansion Rate vs. Defect Size

In S05 (Sample 05), for the constant radial expansion tests, it was attempted to lessen this initial defect by barely retracting (<2mm) the beveled needle tip (shown in

Figure 3-4). However, the larger diameter needle combined with the presence of the bevel still dominated why this initial defect size was larger. Fortunately, regardless of this initial defect size, it was demonstrated that equivalent stretch rates over a certain Pressure to Elastic Modulus (P/E) ratio (important for capturing the entire viscoelastic behavior of the material) could be achieved utilizing all three of the needle types tested (Figure 3-5).

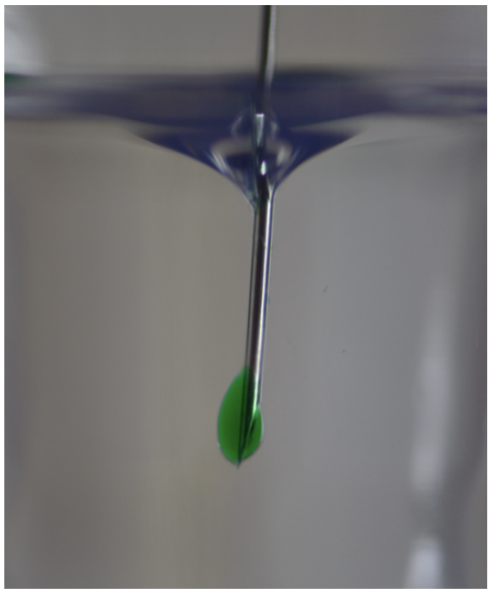

Figure 3-4: Minimal Retraction of Beveled Needle in PDMS

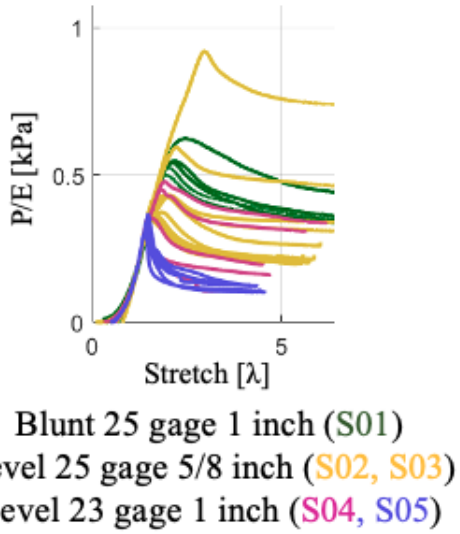

Figure 3-5: Needle Comparison Tests for Constant Radial Tests in PDMS: Stretch vs. Pressure/Elastic Modulus

In both types of expansion tests, it was observed that the cavity placement relative to the needle opening did expand further up the beveled needle than the blunt needle tests as Roth [62] alluded to in her initial work. However, the shape of the expanded fluid cavity was visually observed to be nearly spherical regardless of the needle tip shape (Figure 3-6).

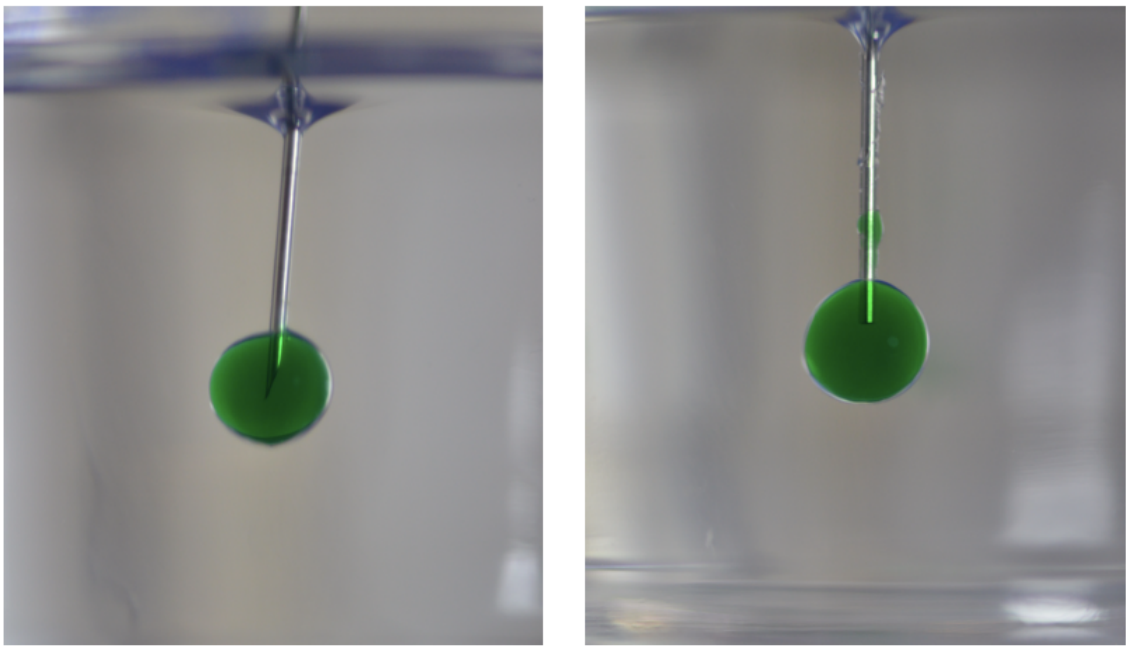

Figure 3-6: Location of Cavity Expansion in Beveled vs. Blunt Needles in PDMS

In conclusion, for a synthetic material such as PDMS, VCCE could be performed to achieve repeatable pressure profile behavior for either a beveled or blunt needle. The length of the needle was not observed to have a significant impact on testing results, most likely due to the relative height of sample to work with and that the needle penetration depth could be kept constant without issue of the needle syringe assembly interference. It was also observed that a larger diameter needle and the presence of a bevel created a larger initial defect. Although, the cavity expansion occurred slightly farther up the beveled needle than in the base scenario of using a blunt needle, this do not appear to significantly impact achieving a pressure profile that included the key features of interest.

3.3.2 Bovine Blood Clots

The procedure for creating, storing and clotting whole bovine blood was same as described in Varner et al.'s work [37]. In these experiments, a 1" 23G beveled, 1" 25G beveled and blunt version, needles were utilized. On the Instron testing device, a CVE test of 2.684mm^3/s was performed with the 23G 1" beveled needle and 25G 1" blunt needle as well as CRE tests at rates of 0.02 and 0.32mm/s for 1" 23G beveled needle only, and 0.08 and 0.64 mm/s for the 1" 25G beveled needle. As similar observations

were noted for both CVE and CRE tests on the Instron, only the CVE graphic results are shown below (Figure 3-7).

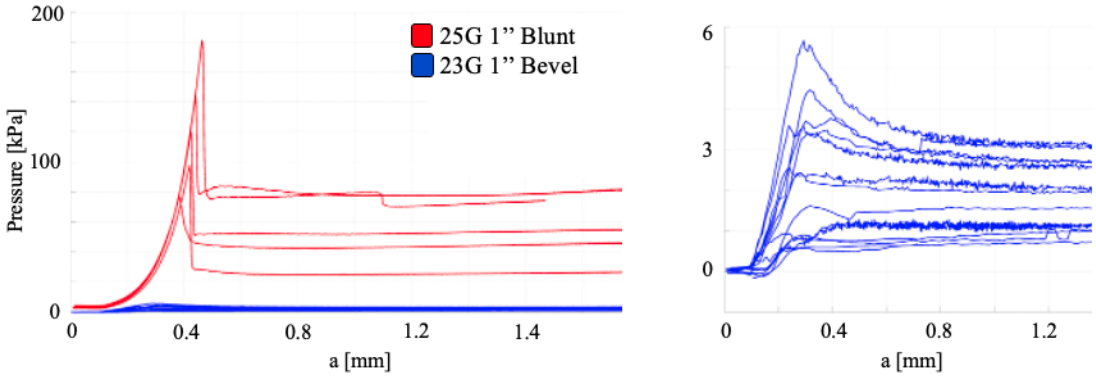

Figure 3-7: Beveled vs. Blunt Needles performing CVE Tests in Blood Clots Utilizing the Instron Device

As previously supported by [37], elastic expansion was achievable with the blunt needle and the critical pressures were within a similar range to those observed in prior tests. The left graph in Figure 3-7 displays both the beveled and blunt needle tests overlaid on one another to show that for the beveled needle experiments, the critical pressures observed were much lower than prior experiments conducted with a blunt needle (<6kPa) and the elastic expansion was minimal with less than half the tests showing expansion beyond the region of 0.1 to 0.2mm (the beveled needle tests are shown again in the right most plot).

Additionally, some bovine blood clots were tested with the GPRT as this tool came online while the needle comparison tests in blood clots were being conducted on the Instron. However, of note, as the syringe size was smaller than the Instron syringe and the maximum injection rate was lower, the rates of the CVE tests that were performed initially utilizing the Instron could not be replicated on the GPRT. The CVE test performed on blood clots using the GPRT was $0.6mm^3/s$. The types of needles used to perform these tests were reduced to only the 1", 25G blunt and beveled needles. It was also attempted to perform CRE tests on the GPRT with both the beveled and blunt needle but as previously alluded to, while attempting to conduct this type of test, it was observed that the pressure profile during injection did not display the key elastic expansion and peak critical pressure at fracture features (Figure 3-8, CRE tests shown in blue in left plot and purple in right plot, respectively).

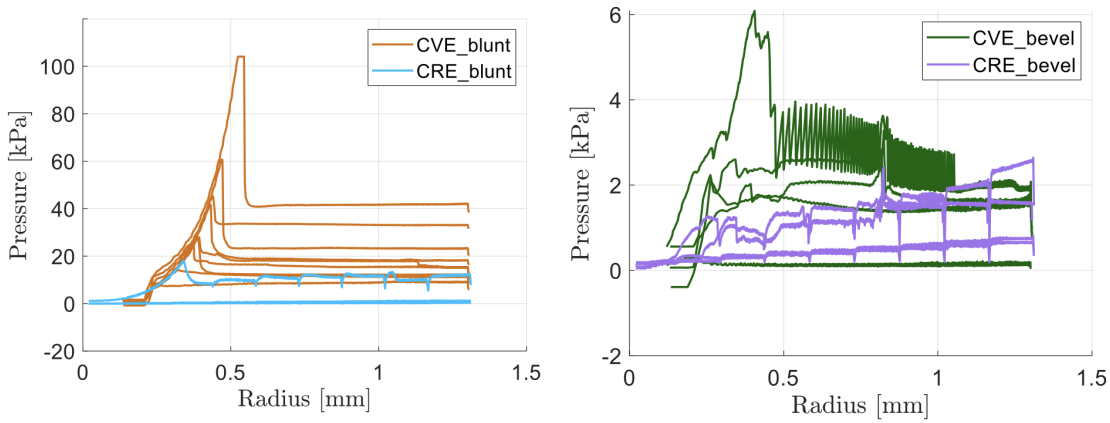

Figure 3-8: Beveled vs. Blunt Needles performing CVE and CRE Tests in Blood Clots Utilizing the GPRT

In conclusion, beveled needles are not recommended for use in blood clots because the maximum critical pressure was much lower than observed in prior testing in blood clots with a blunt needle and the elastic expansion only occurred during a radial expansion period of up to 0.2mm.

3.4 Refining the VCCE Protocol in Previously Untested Biological Materials

As beveled needles proved to enable mixed success in previously tested materials, it was desired to continue attempting to use these needle tips in follow-on tests on biological materials not previously tested with the VCCE protocol. However, in these tests, all other characteristics of the needle (such as length and gauge, 1" and 25G, respectively) were kept constant except for the presence of a bevel or not. For these experiments, further observations regarding the testing protocol alterations were made as well as general observations about the how the key elements of the pressure profile differed for these biological materials.

3.4.1 Bovine Liver

The next biological tissue selected for testing was liver since it possesses a relatively simple tissue structure as compared to other bodily organs. 1 pound of Bovine frozen liver was retrieved from a local butcher store and placed in a refrigerator to thaw overnight. The sample was then cut into 6 centimeters by 5 centimeters sample pieces placed into separate baggies. This size of liver easily fit into petri dishes used to hold samples during testing, as shown in Figure 3-9. On each new day of testing, one liver piece sample was removed from the refrigerator 45 minutes to 1 hour before beginning the testing procedure to ensure the sample had warmed to room temperature

(approximately 22°C). All testing of this material was performed on the GPRT as this was the dedicated device for all future biological tissue testing. Testing was limited to 1 hour (8 to 10 tests) because the sample became noticeably sticky (adhering to needle more easily) after this period of time.

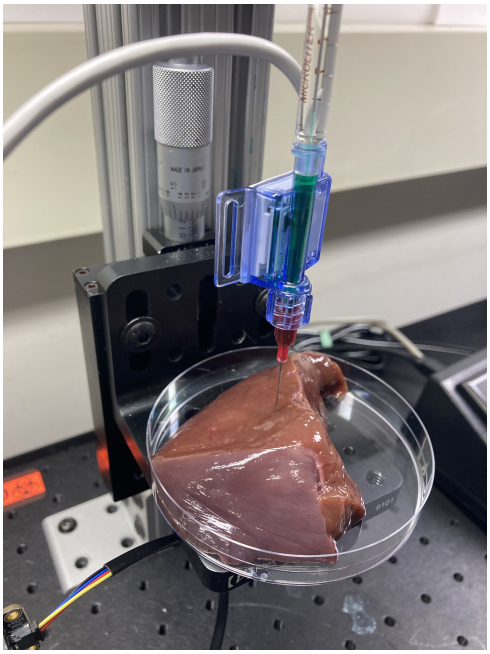

Figure 3-9: Blunt Needle in Bovine Liver

For these experiments, a CVE test rate of 0.6mm^3/s was used for all tests as this rate was demonstrated to constantly achieve the desired pressure profile in blood clots. Both blunt and beveled needles could easily pierce the surface of the liver, however, as shown in Figure 3-10, which displays tests from the same day and sample test, elastic expansion was achieved more consistently using a blunt needle (right plot).

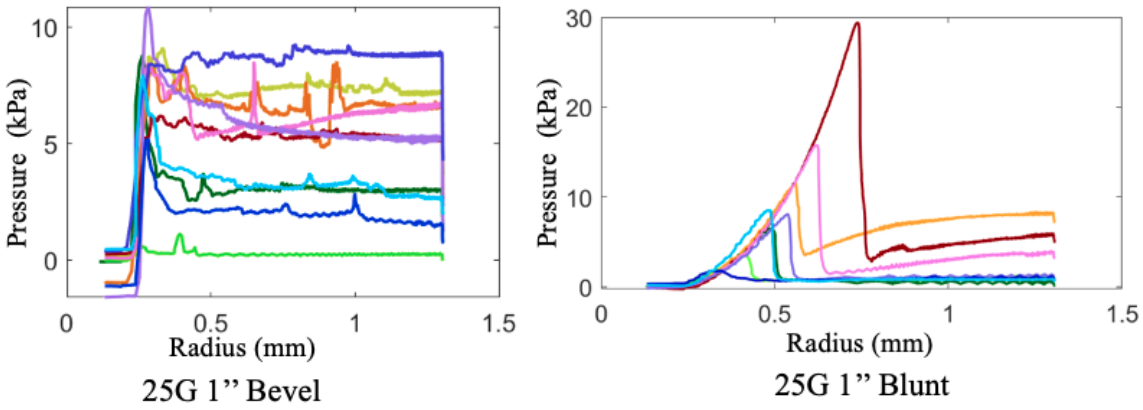

Figure 3-10: Blunt versus Beveled Needle Comparison for Constant Volume Expansion Tests Conducted in Bovine Liver

Additionally, a key observation from these tests was a relatively consistent insertion and retraction distance could be replicated in each bovine liver test which would result in an repeatable pressure profile during this initial step. The actual values of those distances, however, were closer to prior PDMS tests than the bovine blood clots [37]. To develop this consistent retraction and insertion protocol in bovine liver, the pressure response after penetrating a set distance into the material (once the surface of the material is broken, a positive pressure spike is observed) and retracting another set distance (where it is observed that the material is no longer being stressed by the needle's presence but also minimizing the size of cavity created beneath the needle's tip where the fluid will be injected) were observed over the course of 2 to 3 initial tests. For insertion, a distance of 8mm to 1cm was utilized before retracting the needle approximately 3 to 4mm. The peak pressure observed during insertion was typically between 1 to 3 kPa before dropping to ≈ 0 kPa when the needle was retracted. An exception to these peak values were the bovine samples that had aged for 8 days, in this case, the peak insertion pressures were consistently higher (5 to 9kPa). It is hypothesized that this was due to the material aging as it is predicted that it would take more force to rupture the surface as the material is drying out. Of note, there was no notable correlation between the peak insertion pressure and critical pressure at fracture (Figure 3-11).

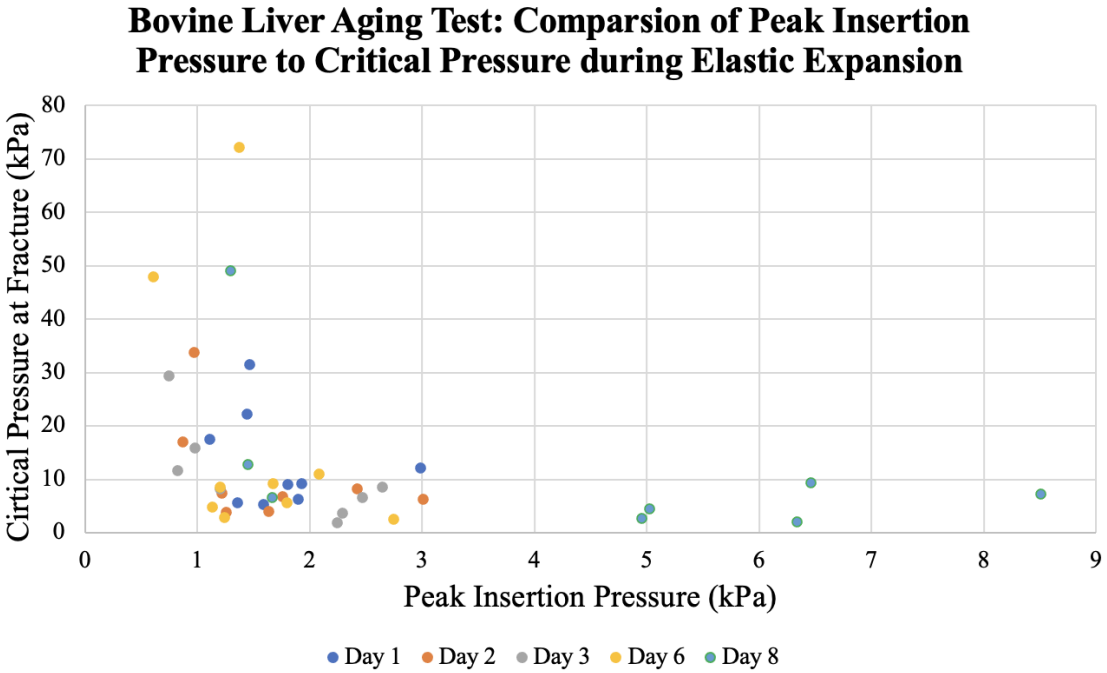

Figure 3-11: Bovine Liver Aging: Peak Pressure vs. Critical Pressure at Fracture

Once the insertion and retraction protocol for this particular tissue was further refined, even greater precision in the elastic expansion region of the pressure profile curve during injection could be achieved for the same sample. Figure 3-12 shows the overlay of a bovine liver aging experiment where multiple elastic expansion profiles are shown, grouped by day of testing. Furthermore, over these 8 days, only one test was

observed to leak visually. Most promising from this particular plot, is the steepening of the exponential elastic branch as the liver "ages". This is indicative of stiffening behavior which is anticipated for a material that is left out of the body for increasing periods of time since the tissue will dehydrate and the structure will begin to break down.

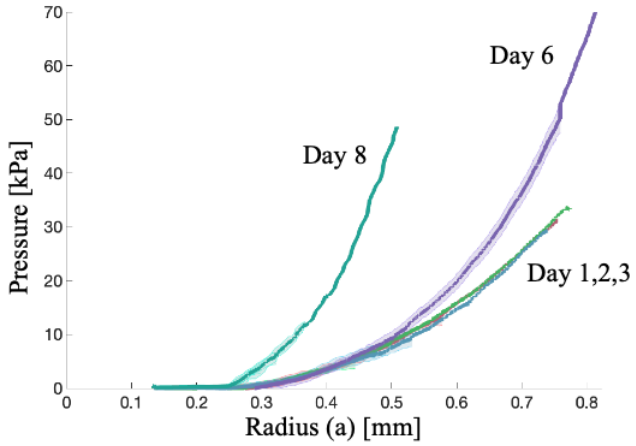

Figure 3-12: Bovine Liver Aging Tests with 25G 1" Blunt Needle

Based on these results, it was concluded that although a blunt or beveled needle could achieve elastic expansion in bovine liver, a blunt needle will provide more consistent values for the key features of the pressure profile as previously identified. Additionally, for this less complex tissue, the protocol for the respective insertion and retraction distances could be established and relatively consistent pressure profiles for both the insertion and retraction step as well as injection step of the VCCE process were achievable.

3.4.2 Swine Thyroid

Swine thyroid was a tissue of interest as it was the best "substitute" tissue to the desired test case of eventual application to a human thyroid. The general anatomy and size of a swine thyroid is very similar to that of humans but is located in a slightly different region of the neck (see Figure 3-13). The swine thyroid was extracted from recently deceased adult male subjects and initially tested within 4 to 20 hours of extraction. Again, a singular CVE test rate of $0.6\text{mm}^3/\text{s}$ was used.

Initial testing immediately indicated that beveled needles were required to implement the VCCE methodology in swine thyroids because of an outer membrane not found on other similar species, such as humans thyroids. Although the thickness of this membrane is quite small relative to the depth of the sample (Figure 3-14 shows the removal of this membrane) it was impenetrable with the blunt needle, especially at the lower velocity speeds typically used for the insertion step of the VCCE protocol. Figure 3-15 shows an attempt to penetrate the outer membrane of pig thyroid with a bevel (orange) versus blunt (red) needle. Figures A-1, A-2, A-3 show a compilation

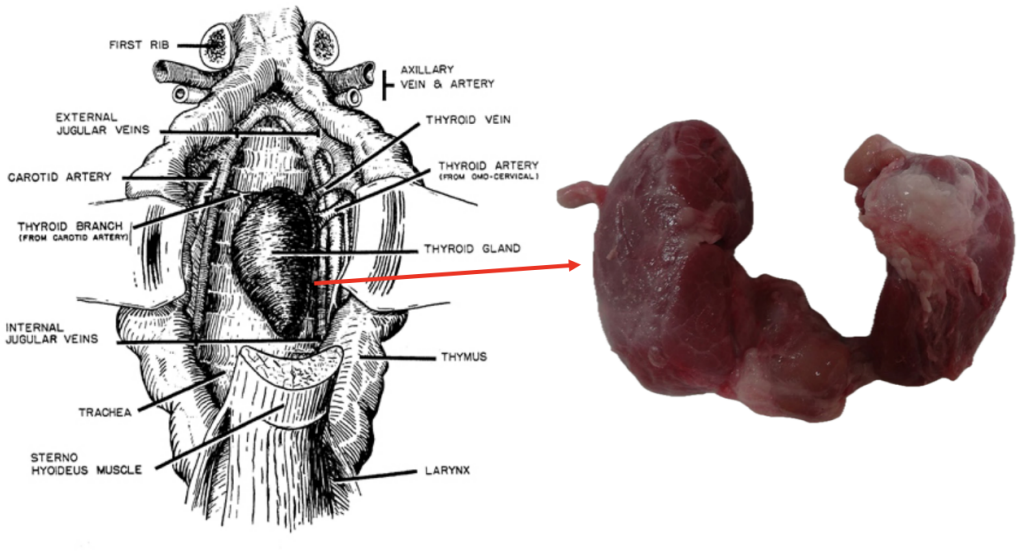

Fig. 3—Schematic drawing of the tissues and anatomical structures in relation to the thyroid gland (ventral view).

Figure 3-13: Swine Thyroid Anatomy Drawing (L) [71] and Extracted Pig Thyroid (R) [72]

of all 30 tests conducted on 3 different swine thyroids (the second swine thyroid was tested on two different days). Of these tests, 7 displayed a consistent elastic expansion and the critical pressures seemed reasonable as compared to prior tests in other biological materials.

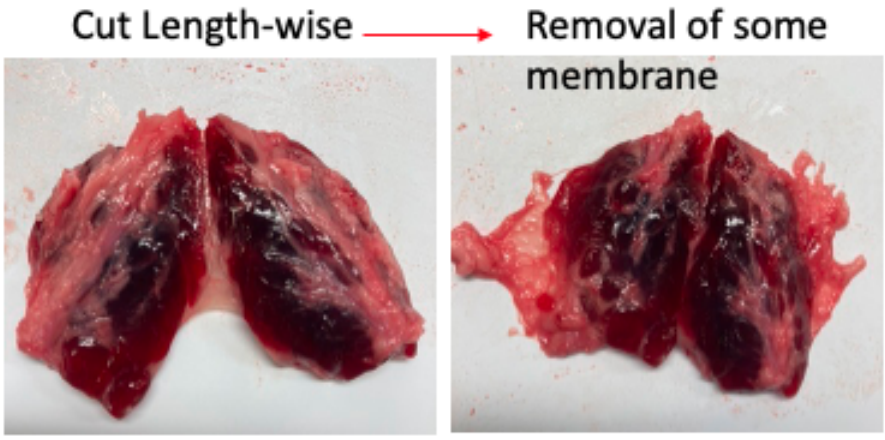

Figure 3-14: Swine Thyroid Membrane Removal

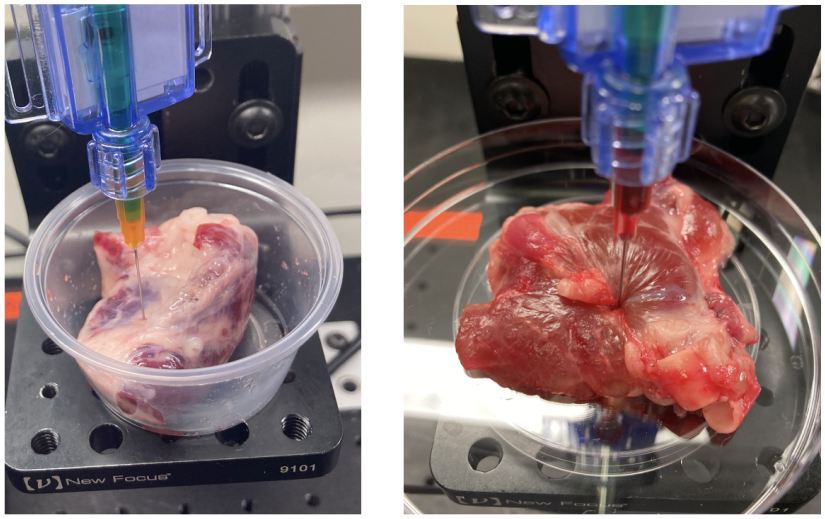

Figure 3-15: Beveled (L) vs. Blunt (R) Tip Needles in Swine Thyroids

It should be noted the insertion and retraction distances varied more greatly while testing in swine thyroids, 5 to 9mm and 1 to 3mm, respectively. The varying insertion distances are hypothesized to be due to the varying difficulty of initial penetration below the surface of these samples. For the retraction distance, it was observed that this tissue surface would not immediately return to a completely non-deformed position when the needle is retracted slightly. This differs from PDMS, blood clots and liver which more easily return to an initial state after needle retraction.

In preparation of nodule testing in extracted human thyroids, it was also attempted to use ultrasound imaging to identify possible nodules in the swine thyroid before beginning VCCE testing. This was demonstrated in a prior study using radiofrequency ablation for swine thyroid nodules [72]. Unfortunately, these attempts proved futile due to the lower image quality, experience of operators in identifying swine anatomy as well as nodule visualization. Additionally, after experiments were conducted on one particular swine thyroid, it was attempted to identify if a nodule of some kind could be identified by dissecting the tissue. As shown in Figure 3-16, there were no clearly identifiable nodules in this sample.

Figure 3-16: Dissection Along Width of Swine Thyroid

Due to the presence of an outer membrane, it was clearly demonstrated that a blunt needle could not be used to penetrate a swine thyroid. Additionally, although a beveled needle was shown as capable of membrane penetration, the difficulty of achieving repeatable pressure profile results indicated that further refinement of the VCCE testing protocol is required for this biological material.

3.5 Final Recommendations

The results of initial needle comparison tests showed that the needle size and presence of bevel were key characteristics to alter in order to achieve the desired pressure profile indicating elastic expansion was achieved. The summary of the recommended needle types are shown in 3.1.

Material	**Needle(s) Tested**	**Conclusion**
PDMS	23G: 1" Beveled, 25G: 5/8" Beveled, 25G: 1" Blunt	Elastic Expansion achievable with all needle types, beveled tip and larger gauge increased initial defect created (but could still achieve similar stretch rates)
Bovine Blood Clots	23G: 1" Beveled, 25G: 1" Beveled and Blunt	Recommend use of blunt needles only, elastic expansion not achievable with beveled needle
Bovine Liver	25G: 1" Beveled and Blunt	Recommend use of blunt needles to consistently achieve elastic expansion
Swine Thyroid	25G: 1" Beveled and Blunt	Beveled needle required to penetrate membrane and elastic expansion can be achieved with this needle type

Table 3.1: Summary of Needle Comparison Tests

Another key conclusion of conducting tests in various types of biological tissues was that the needle insertion and retraction distances had to be altered depending on the tissue of interest because each tissue resisted needle entrance and movement inside the tissue differently. For more homogeneous tissues, such as bovine liver, this procedure could be consistently developed after the first few tests and resulted in more repeatable elastic expansion profiles during the injection phase. However, for more complex tissues such as swine thyroid, this protocol was shown to require further investigation to achieve more consistent pressure results.

Chapter 4

Test Case: Human Thyroid Cancer

In collaboration with Newton Wellesley Hospital, the GPRT was brought into a hospital setting and used to probe extracted human thyroids. The purpose of these tests was to study the challenges with implementing the VCCE methodology in a non-laboratory environment while attempting to collect elastic expansion data on both nodules as well as normal human thyroid tissue. As familiarity with the conduction of this procedure on this tissue improved, the rate of tests where elastic expansion was observed to occur, increased. It was evident from the data gathered during these experiments that VCCE could be implemented to achieve elastic expansion but further refinement of the protocol is needed to improve the precision of these results.

4.1 Background on Study

Newton Wellesley (NW) and Massachusetts General Hospital (MGH) are located in eastern Massachusetts. Every year, over 1,400 thyroidectomies are conducted between both hospitals with a significantly larger share occurring at MGH due to the size of the facilities and staffing. However, all test cases in this initial research study were located at NW. This was because the NW processing system enabled greater flexibility in temporarily diverting a specimen for VCCE testing. Additionally, there was adequate space for the GPRT setup in the pathology suite. In a period of approximately three months (November 2023 to February 2024), 13 of these extracted thyroid cases were tested with the GPRT at NW Hospital. One experimenter conducted each test along with the assistance of one hospital research fellow.

4.2 Hospital Testing Procedure

To transport the GPRT between school laboratory spaces and the hospital, a portable hard-shell case was utilized. To fit the device into this case, the GPRT was deconstructed into the major components. Once reassembled at the hospital, the GPRT could be stored in a portable cart (Figure 4-1) for ease of relocation to another space elsewhere in the hospital when not in use. This cart was outfitted with its' own electrical strip to condense the GPRT's electrical needs into one outlet requirement.

The cart's bottom storage cabinet provided adequate storage space for the assembled device so as to not require breaking down and rebuilding the device between each test case opportunity. As shown in Figure 4-2, the GPRT could be operated on top of the standalone cart or moved to a nearby desk to create more space for other occupants working in the testing area.

Figure 4-1: GPRT Stored in Portable Cart

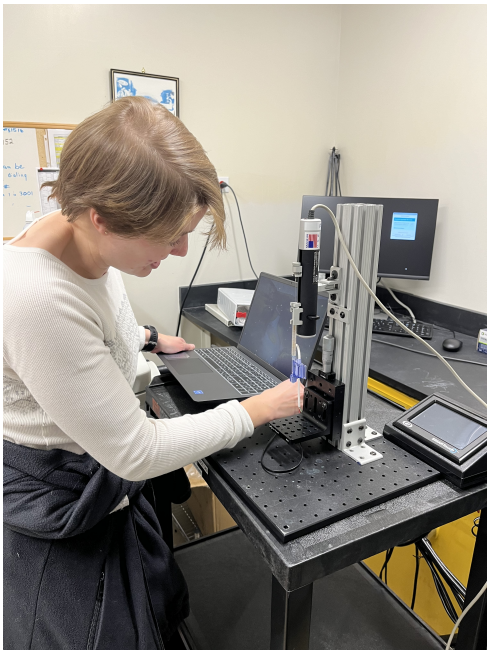

Figure 4-2: GPRT Setup on Portable Cart in Pathology Suite of Newton-Wellesley Hospital

The initial setup of the GPRT required refilling the entire syringe assembly and new needle tip with a 10:1 phosphate buffer solution (PBS) which was exchanged weekly between test cases. To ensure there was was no mechanical or non-mechanical compliance issues in the initial setup, a calibration test was conducted. Once a patient had consented to the study and was anesthetized, a thyroid surgery was found to take anywhere between 2 to 6 hours depending on the size of the thyroid itself and where nodules (benign or cancerous) had spread. If a thyroid was not ready for testing immediately after initial setup, the device was re-calibrated no sooner than 30 minutes before testing on the exracted lobe began.

Approximately 10 to 20 minutes after a thyroid lobe was removed from a patient, the nodule(s) on the thyroid was (were) tested. To locate a nodule of interest, the ultrasound information regarding the location of the suspected nodule and verbal discussions with the surgeon and/or pathologists, conducting the diagnostic testing, were consulted. This was an important consideration for testing especially if the nodule was not visible on the surface of the lobe. To understand the orientation of the nodule within an extracted specimen, the following terminology as described in Figure 4-3 was utilized. After initial processing of the extracted specimen in the pathology suite, it was placed in formalin before being ultimately stored in another hospital location. At this final stage of processing, the lobes and nodules were measured again manually. The average differences between the ultrasound and manual measurements (for each direction of measurement) are shown in Figure 4-4.

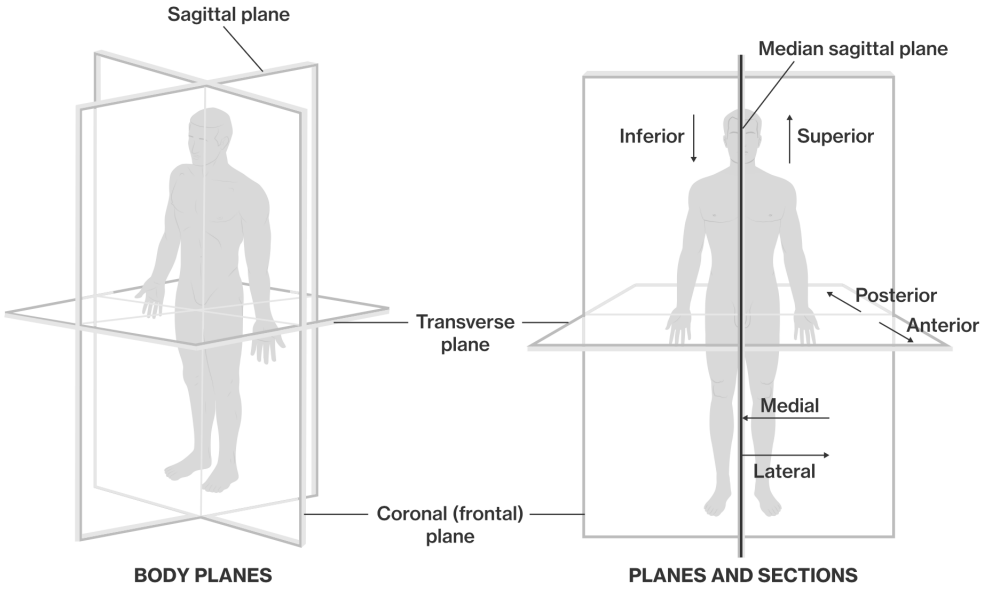

Figure 4-3: Terminology Utilized for Describing Body Planes and Sections

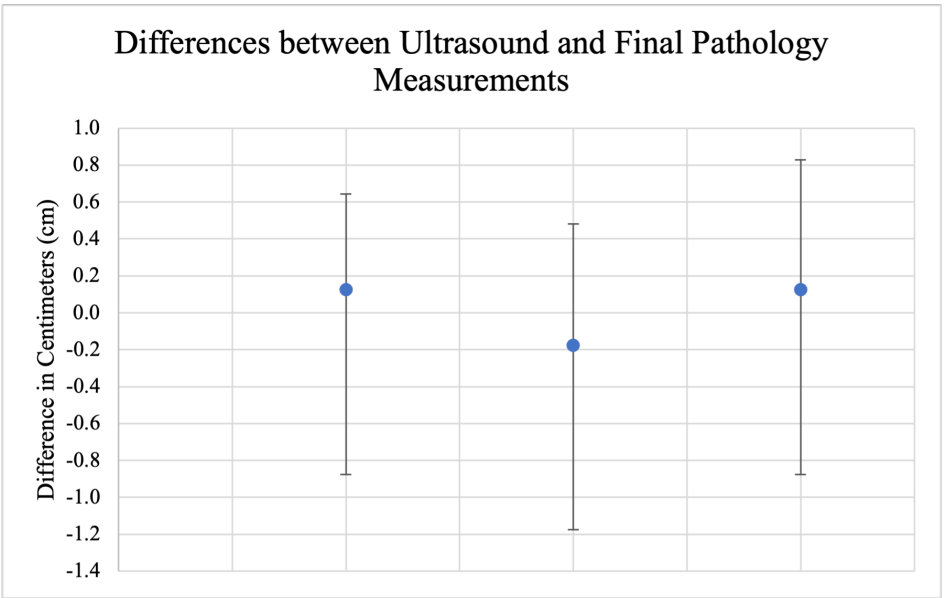

Figure 4-4: Differences between Ultrasound and Final Pathology Measurements

Once the location of the nodule(s) was(were) identified, the insertion step was conducted. As will be discussed in the next section, this insertion depth varied between samples due the range in resistance to needle penetration. Once the nodule was believed to have been penetrated (verified visually and from the pressure readout), the needle tip was inserted 3 to 4 mm further to ensure the needle tip was fully beyond the nodule surface. Then the needle was retracted 1 to 2 mm before beginning the VCCE testing injection procedure. The thyroid specimen was placed back into a temporary storage container between each test in an attempt to slow the dehydration process. After each test, the needle was flushed with a bleach solution before refilling the syringe assembly with the PBS solution. Before testing in normal tissue, the needle tip was exchanged and the calibration was rerun.

If both lobes were to be removed in one patient, this potentially resulted in a 1 to 2 hour break between when the first lobe and second lobe were tested. Testing was desired to be conducted within 60 to 90 minutes of initial extraction so as to minimize any further breakdown of specimen's tissue structure before it was placed in the formalin solution.

4.3 Results

The total time spent testing each case and the corresponding average individual testing time is shown in Figure 4.1. For all cases, these values were also averaged and summarized in Table 4.1. This average testing time closely aligns with the idealized timeline as presented in Section 2.4.1. Figure 4.1 shows a negative linear trend corresponding to a decreasing average time per individual test. This trend was mostly likely due to experimenter becoming more comfortable with the testing procedure and the presence of another person helping with removal and replacement of the specimen

onto the petri dish as well as cleaning and refilling of the needle assembly between tests. Of note, of the 13 test cases, 2 thyroid specimens were too calcified to penetrate with the beveled needle so the testing procedure was not attempted on these samples. These cases were removed from the following plots shown.

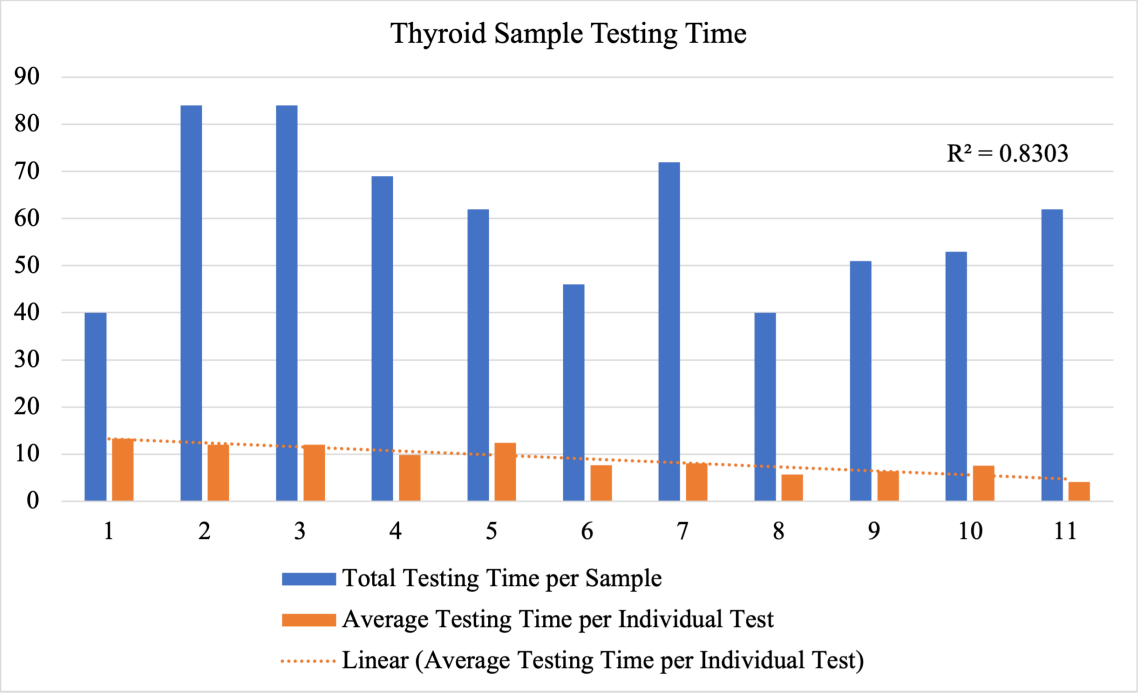

Figure 4-5: Thyroid Sample Testing Time

Total Testing Time with Sample *minutes*	**Average Time per Individual Test** *minutes*
60 ±(16)	9.0 ±(3)

Table 4.1: Average Thyroid Sample Testing Time

To select which tests were suitable for any follow-on analysis such as fitting a material model, the pressure profile during the injection phase was observed for indications that elastic expansion occurred. Other "successful" tests meant the needle penetrated the nodule or normal tissue without touching the bottom of the petri dish and there were no observable leaks during the injection process. The equivalent percentage of successful tests conducted in the nodule versus normal tissue are shown in Figure 4-6.

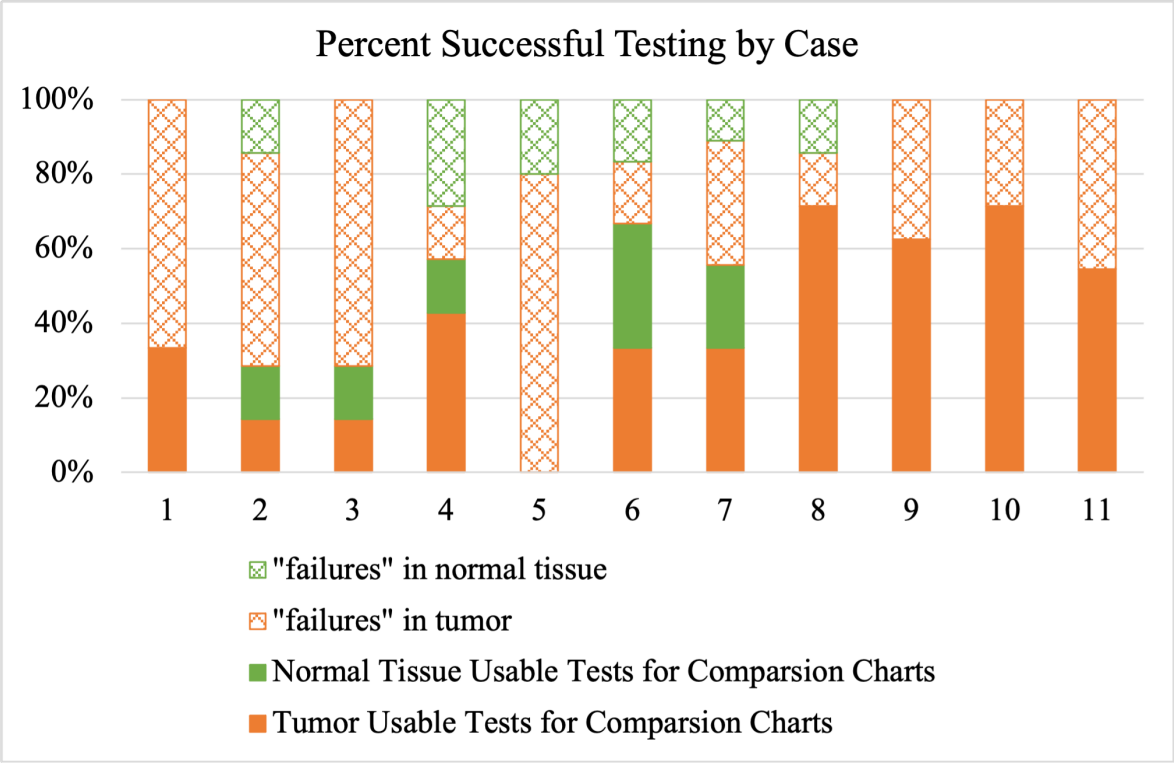

Figure 4-6: Percent Successful VCCE Test by Case

In all test cases, since a lobectomy or thyroidectoctomy was already being conducted, it was more likely the ultimate diagnosis of nodule was malignant since surgery was highly recommended in the first place. Of the 13 test cases, 6 contained malignant nodules while the other 7 were benign. Among the human population, the most common type of thyroid cancer is papillary thyroid carcinoma (PTC) [73]; this was well reflected in the small sample size of test cases studied in this research (all 6 malignant cases were given this diagnosis).

Throughout the course of these experiments, the components of the pressure profile that best differentiated a benign versus normal nodule were explored. In the below plots displayed in Figure 4-7, two examples of extracting key features of VCCE pressure profile in an attempt to help identify the presence of cancer are shown. The left most plot shows a neo-hookean shear modulus fit to the max slope of the elastic expansion curve and the right most plot shows max slope of the pressure versus radius. The symbols represent the corresponding FNA Bethesda scale results and the ultimate diagnosis (as indicated by the benign=orange versus malignant=green tumor categorization). The most encouraging result of this analysis was that the critical pressure and stiffness results collected using the VCCE method also detected that benign nodules given the initial classification of "interdeterminate" were softer than those that were ultimately determined to be malignant.

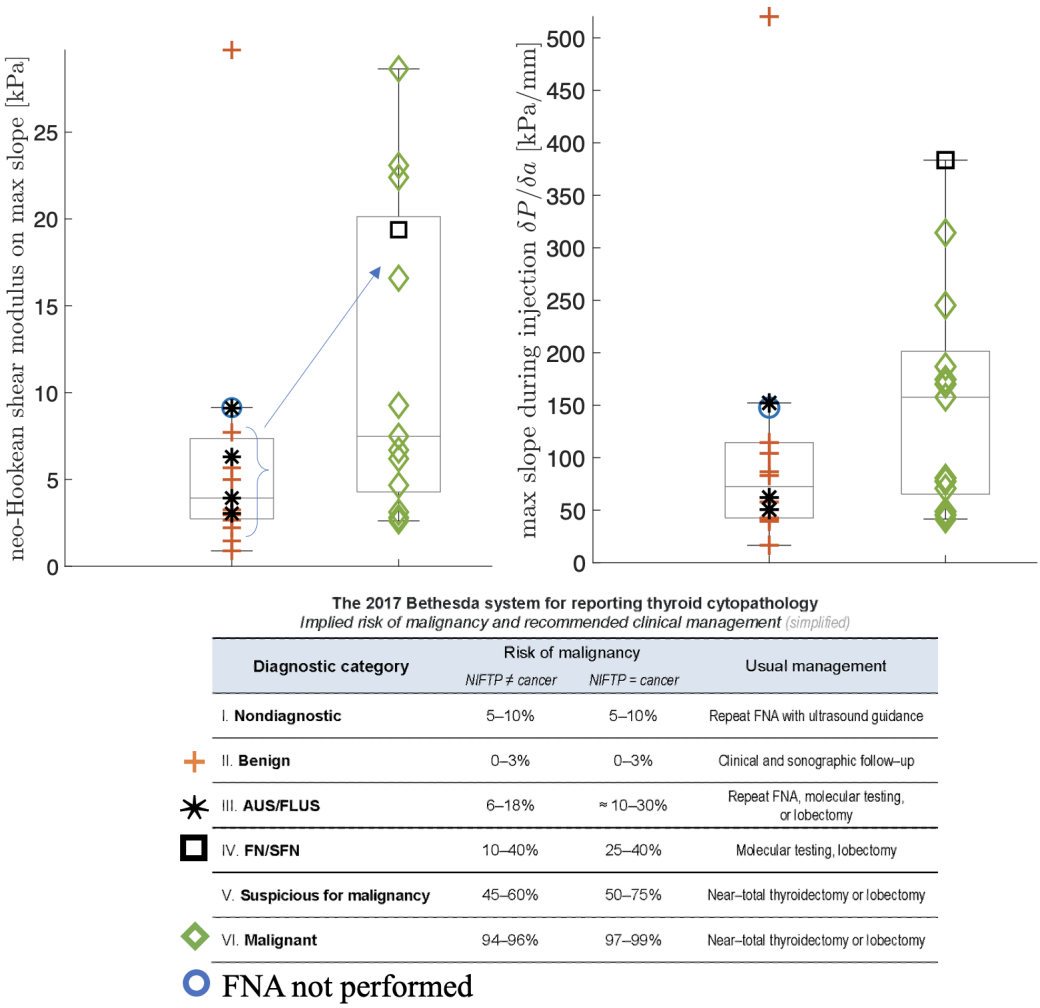

The 2017 Bethesda system for reporting thyroid cytopathology
Implied risk of malignancy and recommended clinical management (simplified)

Diagnostic category	Risk of malignancy		Usual management
	NIFTP ≠ cancer	*NIFTP = cancer*	
I. **Nondiagnostic**	5–10%	5–10%	Repeat FNA with ultrasound guidance
II. **Benign**	0–3%	0–3%	Clinical and sonographic follow-up
III. **AUS/FLUS**	6–18%	≈ 10–30%	Repeat FNA, molecular testing, or lobectomy
IV. **FN/SFN**	10–40%	25–40%	Molecular testing, lobectomy
V. **Suspicious for malignancy**	45–60%	50–75%	Near-total thyroidectomy or lobectomy
VI. **Malignant**	94–96%	97–99%	Near-total thyroidectomy or lobectomy

FNA not performed

Figure 4-7: Bethesda Scale at FNA with Critical Pressure and Stiffness Results Mapped to Final Pathology

4.4 Observed Challenges of Testing and Suggested Improvements

The two greatest difficulties observed during this testing were the variability of nodule size and composition and the accurate identification and availability of "normal" tissue on a lobe to serve as a control reference. As pictures could not be taken in the hospital setting, illustrations were made based of final physical measurements of both nodules and entire lobes (shown in Figure B-2, B-3, B-4, along with a reference picture shown in Figure B-1). The location of the nodules drawn on the lobes are loosely accurate because the main purpose of these drawings to emphasize the general variability of the thyroid lobes and nodules sizes (as well as nodule composition and location relative to the surface of the lobe).

It is widely acknowledged that even a healthy thyroid gland can vary greatly in

size due to varying vasculature and other anatomical differences between persons such as having a pyramidal lobe [74], [75]. This also applies to the variability in nodule size. Figure 4-8 summarizes the range in size of nodules based on dimension as recorded in final pathology (final pathology did consistently measure the final lobe size so it is not shown here). The smallest depth of nodule observed was 0.4 mm, and many lobes contained regions where less than a centimeter of depth was observed. The lack of tissue depth complicated the ability to perform the VCCE test at an adequate distance from the tissue's boundaries.

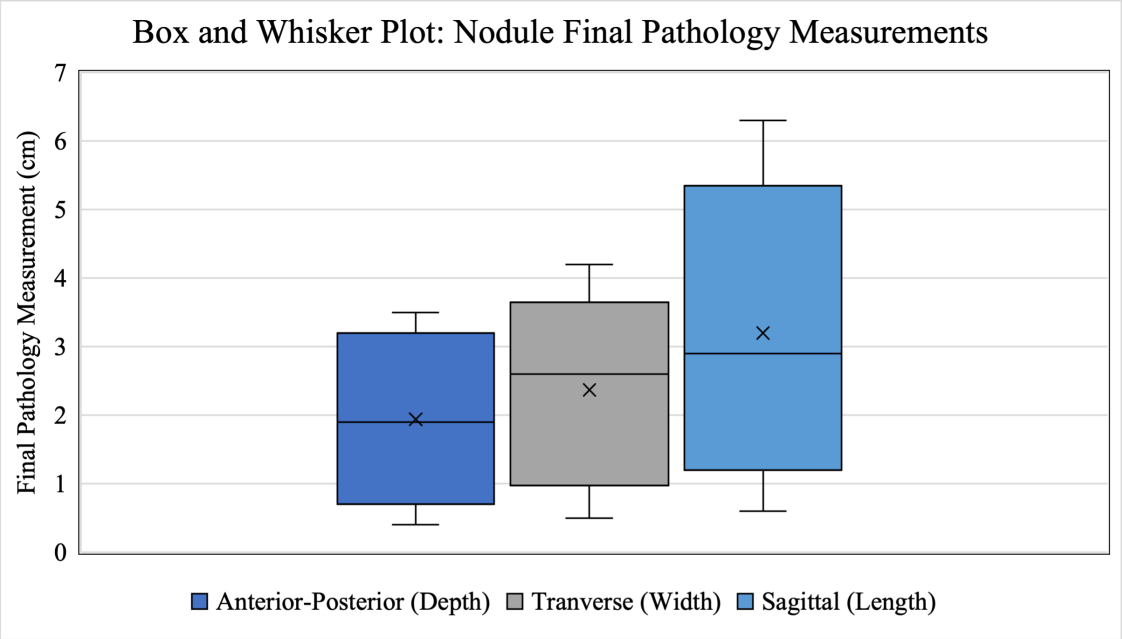

Figure 4-8: Nodule Final Pathology Measurements

For nodules that were exophytic or growing outward from the surface of the lobe, ensuring the needle was penetrating the nodule could easily be verified visually. However, for other nodules that develop beneath the outer surface of the thyroid gland, careful insertion to the nodule's actual location had to be taken. Calcification of a nodule, as previously mentioned, was another condition that made samples impenetrable with the needle being utilized for this initial testing. Additionally, some nodules were also observed to be fluid filled whether with a pus-like substance or blood. Conducting VCCE into fluid bubble would not work because this methodology assumes the mechanical structure resists expansion. If this observation was readily apparent before a test was conducted, this area was avoided but occasionally, this was not discovered until after the needle had penetrated the surface of this nodule.

Initially it was assumed that every thyroid sample would contain enough "normal" tissue to test as a control against VCCE experiments conducted in nodules, however, it was discovered that this would not possible due to the lack of "normal" tissue identified in most samples. Commonly, nodules were found to fully encompassed the entirety of the lobe. In this case, there was too small of a "normal" sample in which the needle could be inserted (not enough vertical height for the needle to be inserted

and retracted while ensuring the fluid cavity is not impacted by boundary conditions). Another common issue encountered was the cauterization of tissue near outer edges of the sample (where the normal tissue was typically located) because this hardens that portion of the tissue, rendering this area too difficult to penetrate with the needle utilized for these experiments.

In future experiments, it is recommended that more careful identification is made as to the precise location of a nodule and normal tissue before beginning every test. This challenge could be alleviated by utilizing ultrasound technology in combination with the insertion and retraction step as it is being actively performed. An ultrasound would similarly aid in identifying areas of the lobe or nodules that are predominantly fluid so as to avoid these areas for direct VCCE fluid injection. FNA procedures have already set the precedent of using such technology in conjunction with the needle insertion procedure to ensure a nodule is being correctly infiltrated. In regards to calcified nodules, these types of nodules have already been identified as notably difficult to test using the traditional needle probing methods according to pathologists consulted during this testing. However, in these cases, it is also more likely that the sample has been diagnosed as malignant before surgery so the need for a methodology that can more accurately diagnose such nodules before thyroid removal is low. As identified in Section 3.1.2, larger diameter or small gauge needles (21 or 22G) should also be explored for implementing VCCE experiments as these needle sizes are already commonly used to perform traditional needle diagnostic procedures in thyroids and may decrease the difficulty of initial penetration into a nodule or normal tissue sample. Additionally, the speed of needle insertion should also be evaluated as the nominal needle-based diagnostic tools employ a faster insertion speed and easily penetrate to the thyroid and associated nodules with repeated success.

Given the variability of tissues and cancerous growths, it is evident that the aid of tools such as in situ ultrasounds to help guide precise needle insertion are vital to improving results gathered using the VCCE methodology. Additionally, it is recommended to investigate the performance of the procedure with larger needle sizes and further refine the insertion and retraction procotol in an effort to obtain more repeatable elastic expansion pressure profile results.

Chapter 5

Conclusions and Future Work

Mechanics play a vital role in both understanding how extreme loading scenarios impact soft-tissued organs but also how diseases such as cancer impact the surrounding microenvironment. Developing methodologies that are able to more consistently and precisely collect material mechanical properties on in-vivo biological tissues, especially under large strain scenarios, are crucial to improving current diagnostic tools for injuries and disease progression. VCCE is a novel, needle-probing methodology for determining mechanical properties of soft materials. This method involves injecting an incompressible fluid into a soft material cavity and monitoring the corresponding pressure as the cavity expands. This technique has been demonstrated successfully in synthetic materials and some ex-vivo biological tissue samples such a murcine brains and bovine blood clots. The purpose of this thesis was to discuss a few of the implementation challenges for utilizing this procedure as an in-vivo, biological tissue, bulk mechanical property testing methodology. This was done through an investigation of needle choice and conducting the VCCE protocol with a miniaturized test set-up on a variety of biological materials with the ultimate application of performing VCCE on extracted human thyroids.

Regarding needle choice, it was desired to investigate how the needle size and presence of bevel impacted the corresponding defect size created during the insertion and retraction portion of the procedure as well as the influence of the needle choice on the elastic expansion pressure profile once the fluid injection step began. The results of this thesis demonstrated that the presence of a beveled tip impacts the defect size more than the diameter of the needle. Additionally, beveled tipped needles were exhibited to have mixed success in achieving elastic expansion in a variety of biological materials. Through the investigation of this procedure on a variety of biological tissues, it was also shown that insertion and retraction protocol needs to be adjusted depending on the material. Furthermore, for materials more homogeneous in nature, the insertion and retraction distances were noted to be more consistent as well as the corresponding peak pressures upon insertion.

The GPRT has allowed the VCCE methodology to transition from a lab only procedure to a bench-top setup in a medical clinic. A current limitation to this tool is its inability to conduct CRE type tests, which in the prior work, has been shown as a necessary to capturing the full viscoelastic behavior of soft materials.

Nevertheless, in this work, it was shown that elastic expansion was achievable in a variety of materials when implementing VCCE using this tool. It is recommended, however, that further comparison tests are conducted in the same materials on the Instron and the GPRT to quantify any differences in the elastic expansion profile between the two testing device set-ups. Another recommended modification to the portable device is to automate control of the velocity of needle as it moves through the material during the insertion and retraction steps. This is currently done manually on both the Instron and GPRT test set-ups which means the resulting speed of insertion and retraction can vary between persons conducting tests or even one person between the conduction of multiple tests.

Conducting VCCE on extracted, diseased human thyroids, exemplified the challenges of working with highly heterogeneous biological tissues. However, these experiments demonstrated that the key features of the pressure profile resulting from a successful VCCE test could still be achieved using the GPRT. Suggested improvements to the results of these experiments would include more precise identification of nodules and more consistent identification and testing of normal thyroid tissue against which to compare a nodule. Additionally, it was noted, that the current speed of insertion associated with the nominal protocol utilized for VCCE meant the initial penetration into the nodule or thyroid surface was very difficult. Current needle based diagnostic tools for thyroid cancers insert the needle much more swiftly, especially to lessen pain imparted to the patient. Future studies are suggested to explore how or if the needle insertion velocity impacts the VCCE pressure profile data once the injection step begins.

As VCCE was applied to a variety of previously un-tested biological materials in this work, it became apparent while analyzing the resulting pressure profile data, that the current material parameter fitting methods may be limited in their specific application. This is why the emphasis of this research was not presenting a specific, calculated mechanical property such as the elastic moduli or stiffness but instead commenting on the achievement of various key features of the VCCE pressure profile. Eventually, it is hoped that a unique, corresponding *local signature* can be generated for each tissue. This signature could then be used for more specific applications such as where disease or injury has infected or impacted a tissue compared to a normal region or compare bulk mechanical properties between different tissues. Further investigation studying the relationship between the key features of the pressure profile during injection will be crucial to clearly identifying a unique tissue and/or its' state of health.

VCCE is an innovative, needle-probing methodology with application to determining mechanical properties of a various biological materials. By perfecting this mechanics-informed in-vivo tissue probing technique, VCCE could be utilized to improve diagnostic tools for damaged and/or diseased tissues, Personal Protective Equipment (PPE), and casualty transport safety guidelines.

Appendix A

Swine Thyroid GPRT Test Results

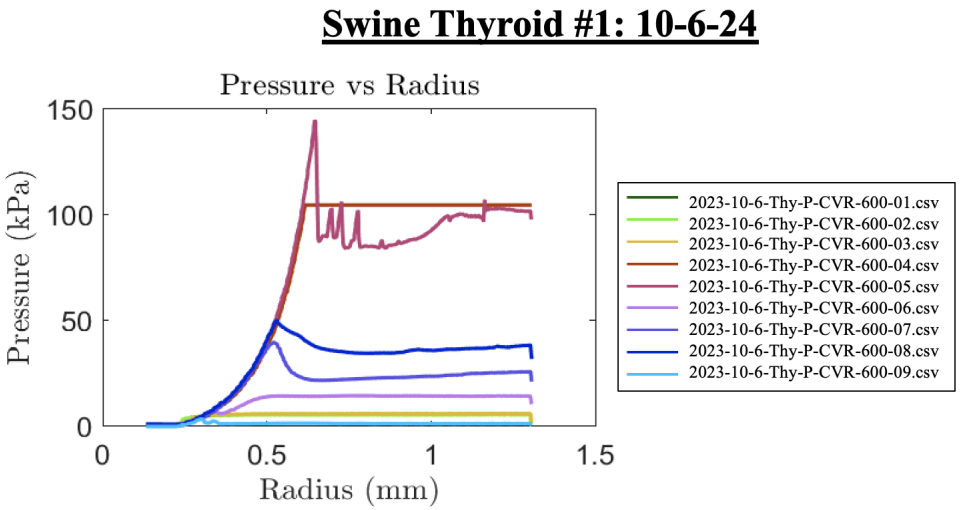

Figure A-1: Swine Thyroid 1 GPRT CVR Tests: Radius vs. Pressure

Swine Thyroid #2: 12-7-24 &12-8-24

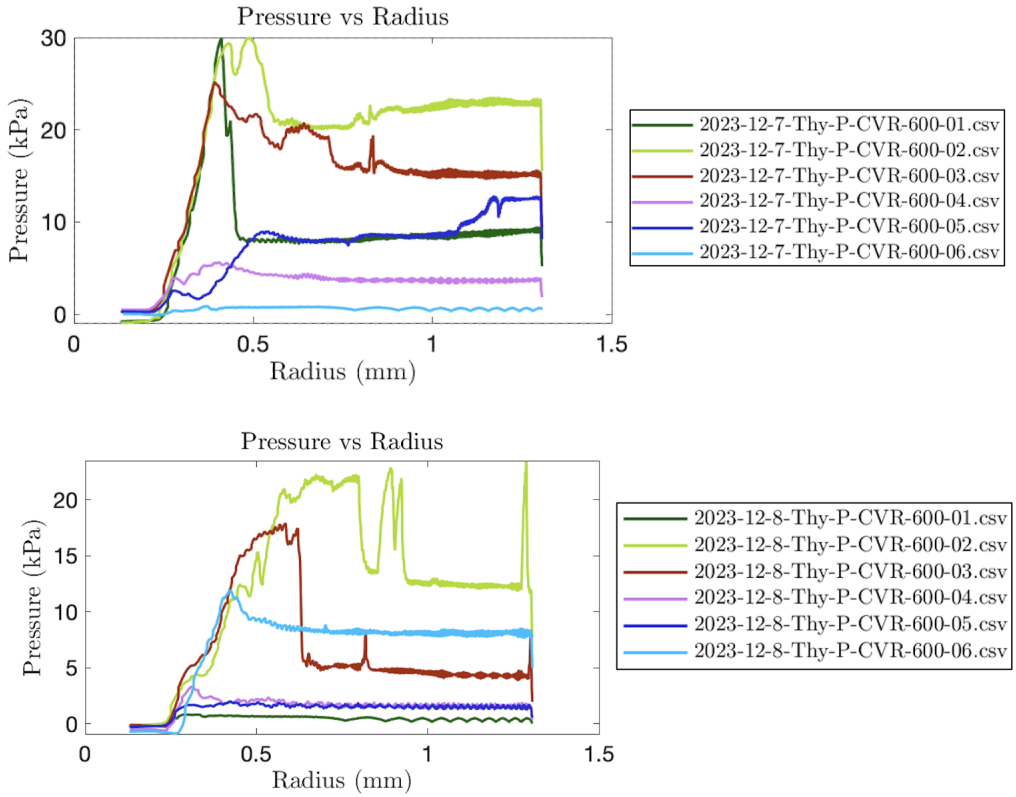

Figure A-2: Swine Thyroid 2 GPRT CVR Tests: Radius vs. Pressure

Swine Thyroid #3: 1-26-24

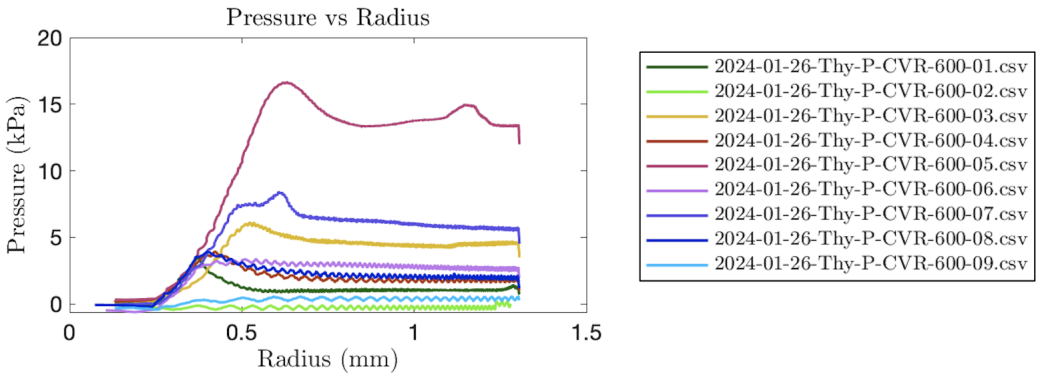

Figure A-3: Swine Thyroid 3 GPRT CVR Tests: Radius vs. Pressure

Appendix B

Illustrations of Extracted Human Thyroids

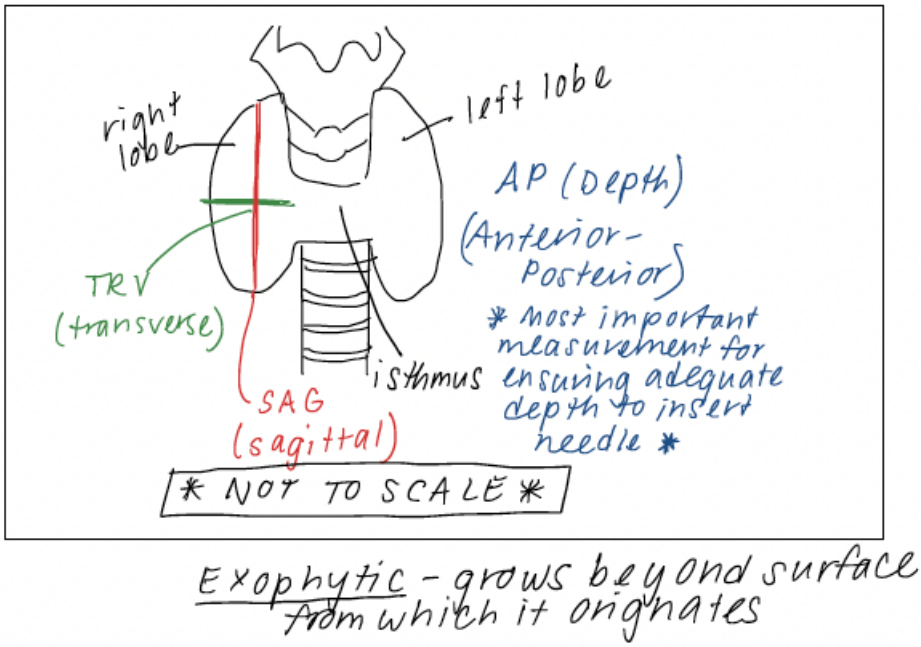

Figure B-1: Legend for Human Thyroid Illustrations: Anatomical Measurements

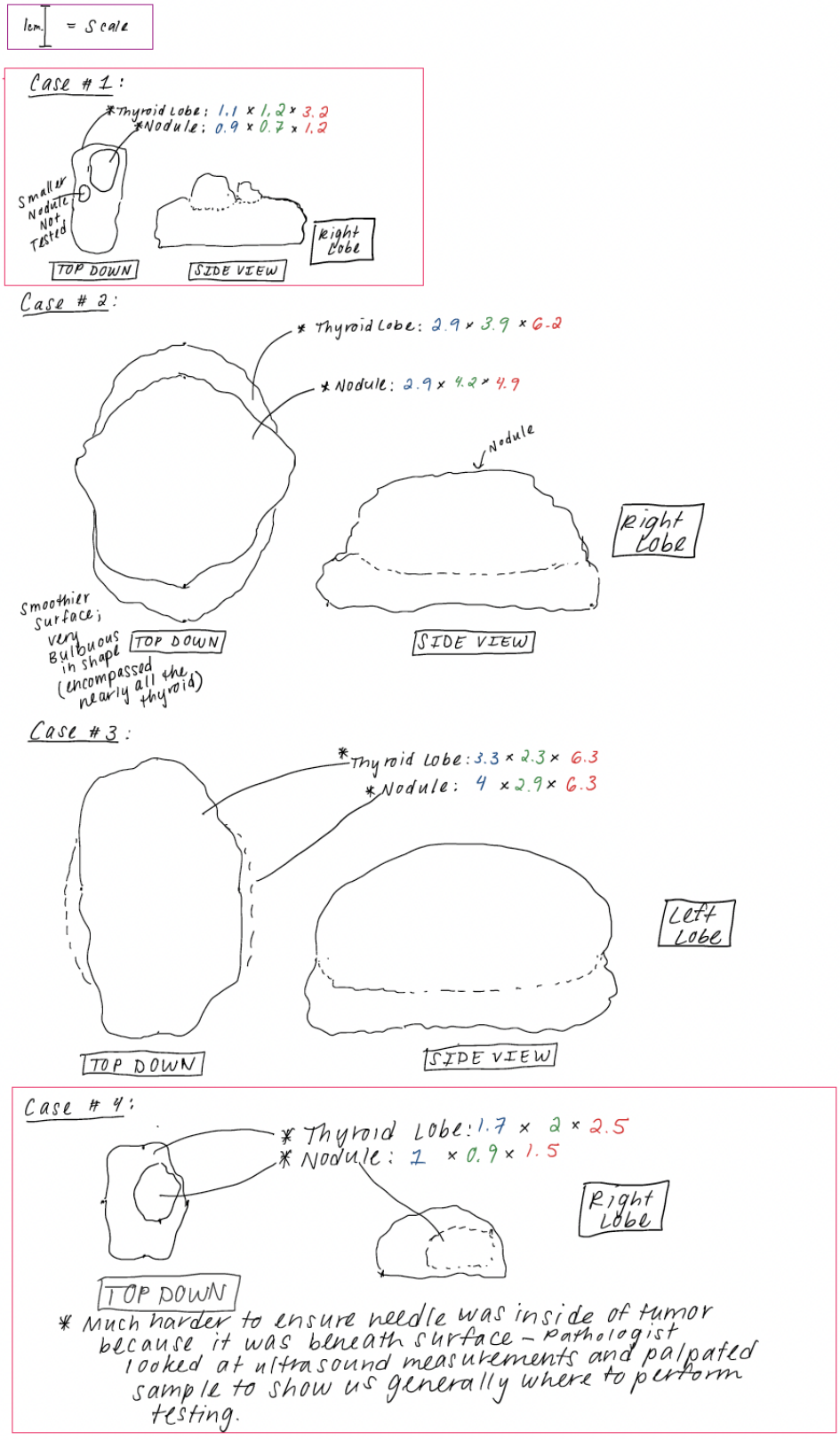

Figure B-2: Human Thyroid Illustrations Test Cases 1-4

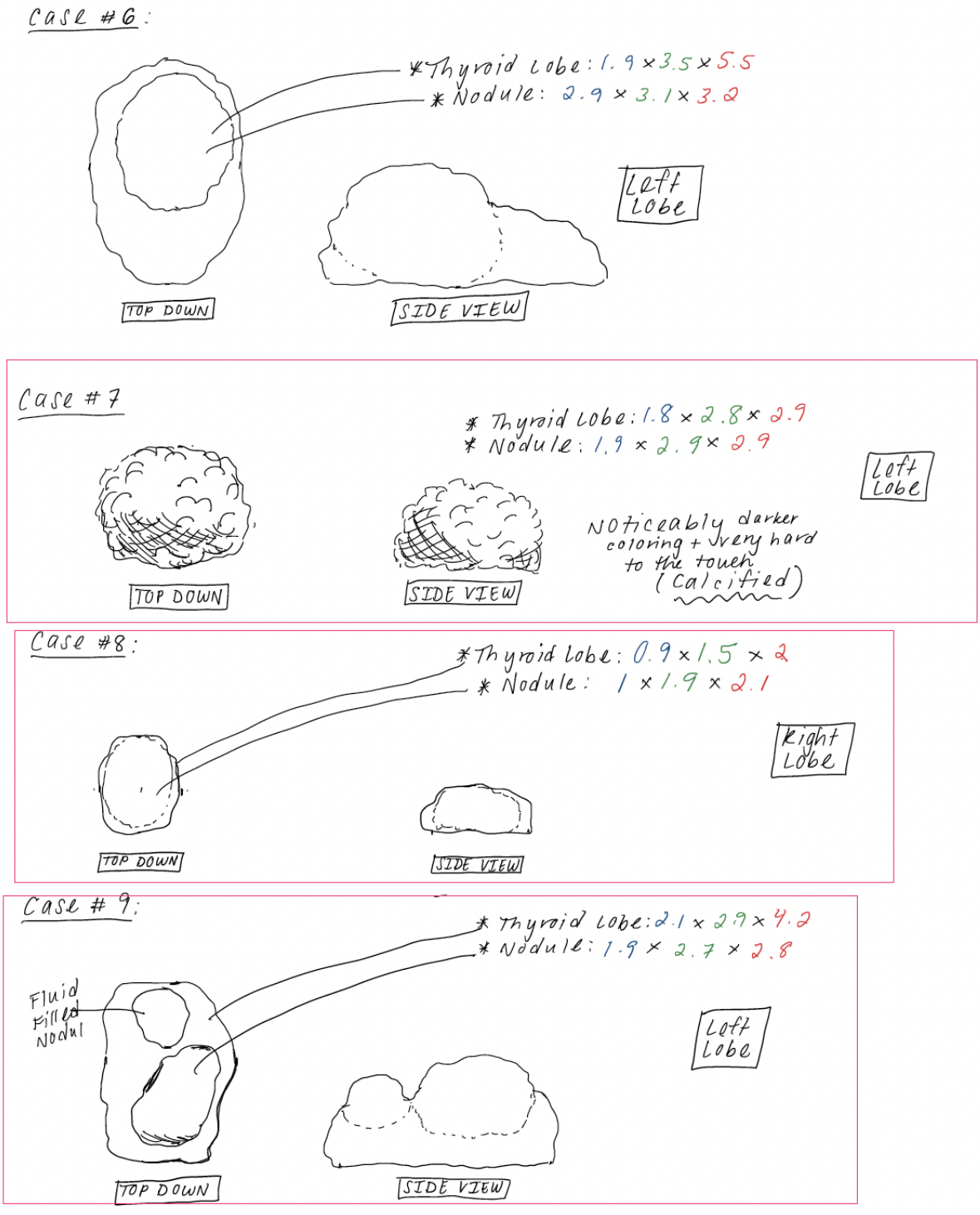

Figure B-3: Human Thyroid Illustrations Test Cases 6-9

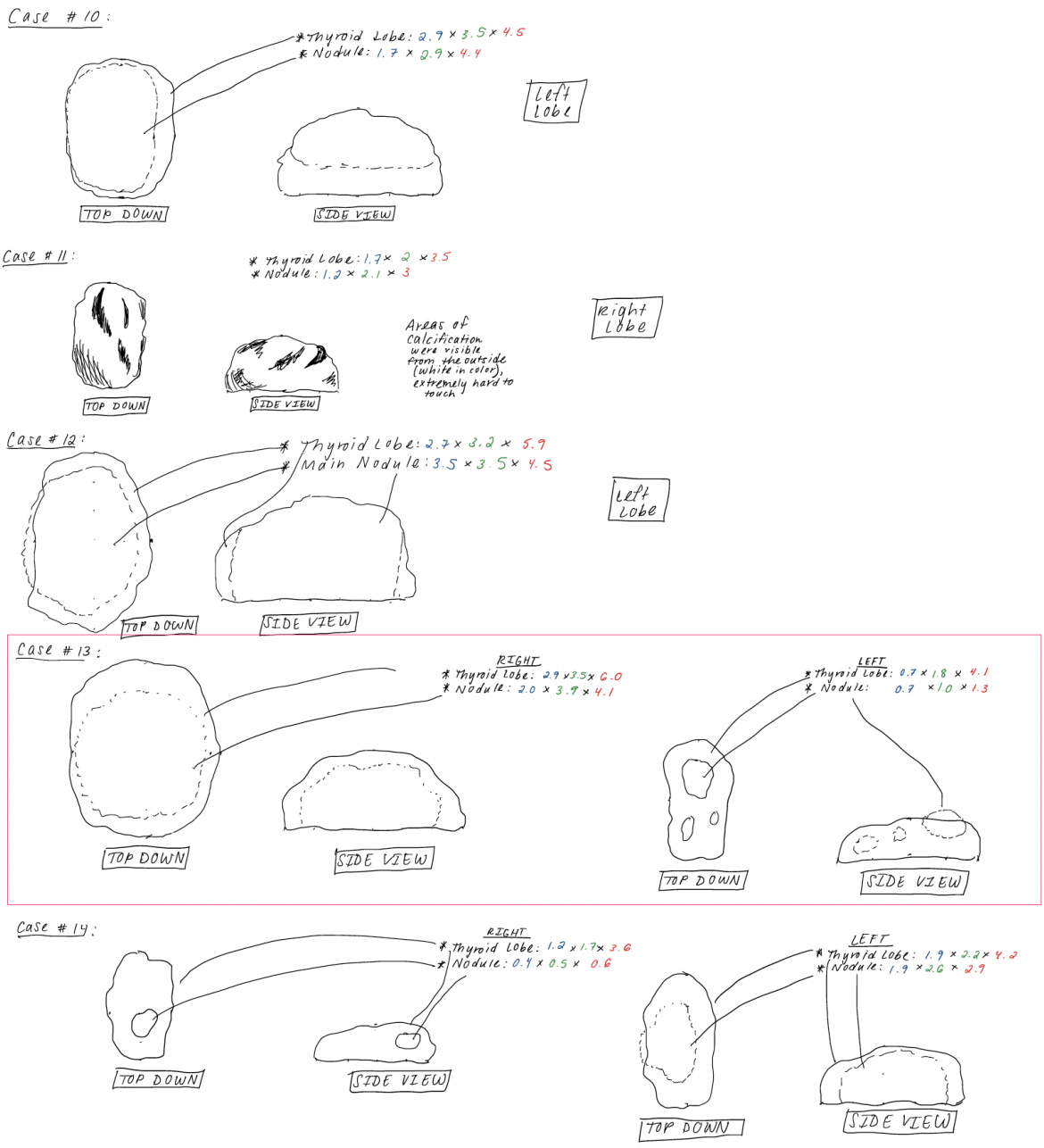

Figure B-4: Human Thyroid Illustrations Test Cases 10-14

Appendix C

List of Acronyms

CRE Constant Radial Expansion

CVE Constant Volume Expansion

CT Computed Tomography

CR Cavitation Rheology

FNA Fine Needle Aspiration

GPRT General Purpose Research Tool

mTBI mild Traumatic Brain Injury

MGH Massachusetts General Hospital

ML Machine Learning

MRI Magnetic Resonance Imaging

NW Newton Wellesley

PDMS Polydimethylsiloxane

PPE Personal Protective Equipment

TBI Traumatic Brain Injury

VCCE Volume Controlled Cavity Expansion

Bibliography

[1] Y. Agimi, L. E. Regasa, and K. C. Stout, "Incidence of traumatic brain injury in the u.s. military, 2010–2014," *Military Medicine*, vol. 184, no. 5, e233–e241, May 1, 2019, ISSN: 0026-4075, 1930-613X. DOI: 10.1093/milmed/usy313. URL: https://academic.oup.com/milmed/article/184/5-6/e233/5230762 (visited on 03/28/2024).

[2] "Traumatic brain injury in the united states: Epidemiology and rehabilitation," Centers for Disease Control and Prevention, Atlanta, GA, Congressional Report, 2015, pp. 2–3.

[3] D. A. Benham, M. C. Vasquez, J. Kerns, K. D. Checchi, R. Mullinax, T. D. Edson, and M. D. Tadlock, "Injury trends aboard US navy vessels: A 50-year analysis of mishaps at sea," *Journal of Trauma and Acute Care Surgery*, vol. 95, no. 2, S41–S49, Aug. 2023, ISSN: 2163-0763, 2163-0755. DOI: 10.1097/TA.0000000000004047. URL: https://journals.lww.com/10.1097/TA.0000000000004047 (visited on 11/17/2023).

[4] L. V. Simon, R. A. Lopez, and K. C. King, "Blunt force trauma," in *StatPearls*, Treasure Island (FL): StatPearls Publishing, 2023. URL: http://www.ncbi.nlm.nih.gov/books/NBK470338/ (visited on 11/17/2023).

[5] C. E. Keating and D. K. Cullen, "Mechanosensation in traumatic brain injury," *Neurobiology of Disease*, vol. 148, p. 105 210, Jan. 2021, ISSN: 09699961. DOI: 10.1016/j.nbd.2020.105210. URL: https://linkinghub.elsevier.com/retrieve/pii/S096999612030485X (visited on 11/17/2023).

[6] E. National Academies of Sciences, H.
bibinitperiod M. Division, B. o. H. C. Services, and C. o. t. R. o. t. D. o. V. A. E. f. T. B. Injury, "MACE 2: Military acute concussion evaluation," in *Evaluation of the Disability Determination Process for Traumatic Brain Injury in Veterans*, National Academies Press (US), Apr. 10, 2019. URL: https://www.ncbi.nlm.nih.gov/books/NBK542592/ (visited on 11/20/2023).

[7] A. C. McKee and M. E. Robinson, "Military-related traumatic brain injury and neurodegeneration," *Alzheimer's & Dementia*, vol. 10, no. 3, Jun. 2014, ISSN: 1552-5260, 1552-5279. DOI: 10.1016/j.jalz.2014.04.003. URL: https://alz-journals.onlinelibrary.wiley.com/doi/10.1016/j.jalz.2014.04.003 (visited on 11/17/2023).

[8] *Evaluation of the disability determination process for traumatic brain injury in veterans*. Washington, DC: The National Academies Press, 2019, OCLC: 1102813345, ISBN: 978-0-309-48686-6.

[9] D. Philipps and M. Callahan, "A secret war, strange new wounds and silence from the pentagon," *The New York Times*, Nov. 5, 2023, ISSN: 0362-4331. URL: https://www.nytimes.com/2023/11/05/us/us-army-marines-artillery-isis-pentagon.html (visited on 11/29/2023).

[10] A. F. Logsdon, B. P. Lucke-Wold, R. C. Turner, J. D. Huber, C. L. Rosen, and J. W. Simpkins, "Role of microvascular disruption in brain damage from traumatic brain injury," in *Comprehensive Physiology*, R. Terjung, Ed., 1st ed., Wiley, Jun. 24, 2015, pp. 1147–1160, ISBN: 978-0-470-65071-4. DOI: 10.1002/cphy.c140057. URL: https://onlinelibrary.wiley.com/doi/10.1002/cphy.c140057 (visited on 03/05/2024).

[11] I. F. Eisenhauer, B. D. Walrath, V. S. Bebarta, M. D. Tadlock, J. B. Baker, and S. G. Schauer, "Navy en-route care in future distributed maritime operations: A review of clinician capabilities and roles of care," *Prehospital Emergency Care*, vol. 27, no. 4, pp. 465–472, May 19, 2023, ISSN: 1090-3127, 1545-0066. DOI: 10.1080/10903127.2022.2107127. URL: https://www.tandfonline.com/doi/full/10.1080/10903127.2022.2107127 (visited on 12/01/2023).

[12] Commander, U.S. 2nd Fleet. "Amphibious assault ships (LHA/LHD)." (), URL: https://www.c2f.usff.navy.mil/Organization/Expeditionary-Strike-Group-ESG-2/Organization/Ships/Amphibious-Assault-Ships/.

[13] Xavier Vavasseur. "Austal USA wings u.s. navy contract for expeditionary medical ship," News. (Dec. 22, 2023), URL: https://www.navalnews.com/naval-news/2023/12/austal-usa-wins-u-s-navy-contract-for-expeditionary-medical-ship/ (visited on 03/04/2024).

[14] "Expeditionary fast transport [t-EPF]," Ships. (), URL: https://www.austal.com/ships/expeditionary-fast-transport-t-epf.

[15] Committee on Diagnostic Error in Health Care, Board on Health Care Services, Institute of Medicine, and The National Academies of Sciences, Engineering, and Medicine, *Improving Diagnosis in Health Care*, E. P. Balogh, B. T. Miller, and J. R. Ball, Eds. Washington, D.C.: National Academies Press, Dec. 29, 2015, Pages: 21794, ISBN: 978-0-309-37769-0. DOI: 10.17226/21794. URL: http://www.nap.edu/catalog/21794 (visited on 03/21/2024).

[16] L. P. Busby, J. L. Courtier, and C. M. Glastonbury, "Bias in radiology: The how and why of misses and misinterpretations," *RadioGraphics*, vol. 38, no. 1, pp. 236–247, Jan. 2018, ISSN: 0271-5333, 1527-1323. DOI: 10.1148/rg.2018170107. URL: http://pubs.rsna.org/doi/10.1148/rg.2018170107 (visited on 03/29/2024).

[17] C. S. Lee, P. G. Nagy, S. J. Weaver, and D. E. Newman-Toker, "Cognitive and system factors contributing to diagnostic errors in radiology," *American Journal of Roentgenology*, vol. 201, no. 3, pp. 611–617, Sep. 2013, ISSN: 0361-803X, 1546-3141. DOI: 10.2214/AJR.12.10375. URL: https://www.ajronline.org/doi/10.2214/AJR.12.10375 (visited on 03/29/2024).

[18] A. Pavlou, R. M. Kurtz, and J. W. Song, "Diagnostic accuracy studies in radiology: How to recognize and address potential sources of bias," *Radiology Research and Practice*, vol. 2021, A. L. F. Costa, Ed., pp. 1–10, Sep. 6, 2021, ISSN: 2090-195X, 2090-1941. DOI: 10.1155/2021/5801662. URL: https://www.hindawi.com/journals/rrp/2021/5801662/ (visited on 03/29/2024).

[19] E. K. Pillai and K. Franze, "Mechanics in the nervous system: From development to disease," *Neuron*, S0896627323007596, Nov. 2023, ISSN: 08966273. DOI: 10.1016/j.neuron.2023.10.005. URL: https://linkinghub.elsevier.com/retrieve/pii/S0896627323007596 (visited on 12/04/2023).

[20] S. Budday, G. Sommer, C. Birkl, *et al.*, "Mechanical characterization of human brain tissue," *Acta Biomaterialia*, vol. 48, pp. 319–340, Jan. 2017, ISSN: 17427061. DOI: 10.1016/j.actbio.2016.10.036. URL: https://linkinghub.elsevier.com/retrieve/pii/S1742706116305633 (visited on 03/21/2024).

[21] A. N. Natali, E. L. Carniel, and H. Gregersen, "Biomechanical behaviour of oesophageal tissues: Material and structural configuration, experimental data and constitutive analysis," *Medical Engineering & Physics*, vol. 31, no. 9, pp. 1056–1062, Nov. 2009, ISSN: 13504533. DOI: 10.1016/j.medengphy.2009.07.003. URL: https://linkinghub.elsevier.com/retrieve/pii/S1350453309001453 (visited on 03/06/2024).

[22] S. Halder, J. Yamasaki, S. Acharya, W. Kou, G. Elisha, D. A. Carlson, P. J. Kahrilas, J. E. Pandolfino, and N. A. Patankar, "Esophageal virtual disease landscape using mechanics-informed machine learning," *Artificial Intelligence in Medicine*, vol. 134, p. 102 435, Dec. 2022, ISSN: 09333657. DOI: 10.1016/j.artmed.2022.102435. arXiv: 2111.09993[physics]. URL: http://arxiv.org/abs/2111.09993 (visited on 12/04/2023).

[23] H. T. Nia, L. L. Munn, and R. K. Jain, "Physical traits of cancer," *Science*, vol. 370, no. 6516, eaaz0868, Oct. 30, 2020, ISSN: 0036-8075, 1095-9203. DOI: 10.1126/science.aaz0868. URL: https://www.science.org/doi/10.1126/science.aaz0868 (visited on 03/02/2024).

[24] S. Ishihara and H. Haga, "Matrix stiffness contributes to cancer progression by regulating transcription factors," *Cancers*, vol. 14, no. 4, p. 1049, Feb. 18, 2022, ISSN: 2072-6694. DOI: 10.3390/cancers14041049. URL: https://www.mdpi.com/2072-6694/14/4/1049 (visited on 03/21/2024).

[25] A. Evans, P. Whelehan, K. Thomson, K. Brauer, L. Jordan, C. Purdie, D. McLean, L. Baker, S. Vinnicombe, and A. Thompson, "Differentiating benign from malignant solid breast masses: Value of shear wave elastography according to lesion stiffness combined with greyscale ultrasound according to BI-RADS

classification," *British Journal of Cancer*, vol. 107, no. 2, pp. 224–229, Jul. 2012, ISSN: 0007-0920, 1532-1827. DOI: 10.1038/bjc.2012.253. URL: https://www.nature.com/articles/bjc2012253 (visited on 03/21/2024).

[26] M. Shahryari, H. Tzschätzsch, J. Guo, *et al.*, "Tomoelastography distinguishes noninvasively between benign and malignant liver lesions," *Cancer Research*, vol. 79, no. 22, pp. 5704–5710, Nov. 15, 2019, ISSN: 0008-5472, 1538-7445. DOI: 10.1158/0008-5472.CAN-19-2150. URL: https://aacrjournals.org/cancerres/article/79/22/5704/638717/Tomoelastography-Distinguishes-Noninvasively (visited on 03/21/2024).

[27] O. Rouvière, C. Melodelima, A. Hoang Dinh, F. Bratan, G. Pagnoux, T. Sanzalone, S. Crouzet, M. Colombel, F. Mège-Lechevallier, and R. Souchon, "Stiffness of benign and malignant prostate tissue measured by shear-wave elastography: A preliminary study," *European Radiology*, vol. 27, no. 5, pp. 1858–1866, May 2017, ISSN: 0938-7994, 1432-1084. DOI: 10.1007/s00330-016-4534-9. URL: http://link.springer.com/10.1007/s00330-016-4534-9 (visited on 03/21/2024).

[28] K. Navindaran, J. S. Kang, and K. Moon, "Techniques for characterizing mechanical properties of soft tissues," *Journal of the Mechanical Behavior of Biomedical Materials*, vol. 138, p. 105 575, Feb. 2023, ISSN: 17516161. DOI: 10.1016/j.jmbbm.2022.105575. URL: https://linkinghub.elsevier.com/retrieve/pii/S1751616122004805 (visited on 12/04/2023).

[29] R. L. Reis and S. Weiner, Eds., *Learning from Nature How to Design New Implantable Biomaterialsis: From Biomineralization Fundamentals to Biomimetic Materials and Processing Routes*, vol. 171, NATO Science Series II: Mathematics, Physics and Chemistry, Dordrecht: Springer Netherlands, 2005, ISBN: 978-1-4020-2647-8 978-1-4020-2648-5. DOI: 10.1007/1-4020-2648-X. URL: http://link.springer.com/10.1007/1-4020-2648-X (visited on 04/01/2024).

[30] N. Özkaya, D. Leger, D. Goldsheyder, and M. Nordin, "Mechanical properties of biological tissues," in *Fundamentals of Biomechanics*. Cham: Springer International Publishing, 2017, pp. 361–387, ISBN: 978-3-319-44737-7 978-3-319-44738-4. DOI: 10.1007/978-3-319-44738-4_15. URL: http://link.springer.com/10.1007/978-3-319-44738-4_15 (visited on 03/21/2024).

[31] J. A. Zimberlin, J. J. McManus, and A. J. Crosby, "Cavitation rheology of the vitreous: Mechanical properties of biological tissue," *Soft Matter*, vol. 6, no. 15, p. 3632, 2010, ISSN: 1744-683X, 1744-6848. DOI: 10.1039/b925407b. URL: http://xlink.rsc.org/?DOI=b925407b (visited on 03/29/2024).

[32] C. S. Nickerson, J. Park, J. A. Kornfield, and H. Karageozian, "Rheological properties of the vitreous and the role of hyaluronic acid," *Journal of Biomechanics*, vol. 41, no. 9, pp. 1840–1846, 2008, ISSN: 00219290. DOI: 10.1016/j.jbiomech.2008.04.015. URL: https://linkinghub.elsevier.com/retrieve/pii/S0021929008001917 (visited on 03/29/2024).

[33] G. P. Sugerman, S. H. Parekh, and M. K. Rausch, "Nonlinear, dissipative phenomena in whole blood clot mechanics," *Soft Matter*, vol. 16, no. 43, pp. 9908–9916, 2020, ISSN: 1744-683X, 1744-6848. DOI: 10.1039/D0SM01317J. URL: http://xlink.rsc.org/?DOI=D0SM01317J (visited on 05/24/2023).

[34] F. Malone, E. McCarthy, P. Delassus, P. Fahy, J. Kennedy, A. J. Fagan, and L. Morris, "The mechanical characterisation of bovine embolus analogues under various loading conditions," *Cardiovascular Engineering and Technology*, vol. 9, no. 3, pp. 489–502, Sep. 2018, ISSN: 1869-408X, 1869-4098. DOI: 10.1007/s13239-018-0352-3. URL: http://link.springer.com/10.1007/s13239-018-0352-3 (visited on 03/29/2024).

[35] J. Chueh, A. Wakhloo, G. Hendricks, C. Silva, J. Weaver, and M. Gounis, "Mechanical characterization of thromboemboli in acute ischemic stroke and laboratory embolus analogs," *American Journal of Neuroradiology*, vol. 32, no. 7, pp. 1237–1244, Aug. 2011, ISSN: 0195-6108, 1936-959X. DOI: 10.3174/ajnr.A2485. URL: http://www.ajnr.org/lookup/doi/10.3174/ajnr.A2485 (visited on 03/29/2024).

[36] S. Franchi-Abella, C. Elie, and J.-M. Correas, "Ultrasound elastography: Advantages, limitations and artefacts of the different techniques from a study on a phantom," *Diagnostic and Interventional Imaging*, vol. 94, no. 5, pp. 497–501, May 2013, ISSN: 22115684. DOI: 10.1016/j.diii.2013.01.024. URL: https://linkinghub.elsevier.com/retrieve/pii/S2211568413000326 (visited on 03/29/2024).

[37] H. Varner, G. P. Sugerman, M. K. Rausch, and T. Cohen, "Elasticity of whole blood clots measured via volume controlled cavity expansion," *Journal of the Mechanical Behavior of Biomedical Materials*, vol. 143, p. 105 901, Jul. 2023, ISSN: 17516161. DOI: 10.1016/j.jmbbm.2023.105901. URL: https://linkinghub.elsevier.com/retrieve/pii/S1751616123002540 (visited on 03/04/2024).

[38] C. D. Untaroiu and Y.-C. Lu, "Material characterization of liver parenchyma using specimen-specific finite element models," *Journal of the Mechanical Behavior of Biomedical Materials*, vol. 26, pp. 11–22, Oct. 2013, ISSN: 17516161. DOI: 10.1016/j.jmbbm.2013.05.013. URL: https://linkinghub.elsevier.com/retrieve/pii/S1751616113001781 (visited on 04/12/2024).

[39] E. Bar-Kochba, M. T. Scimone, J. B. Estrada, and C. Franck, "Strain and rate-dependent neuronal injury in a 3d in vitro compression model of traumatic brain injury," *Scientific Reports*, vol. 6, no. 1, p. 30 550, Aug. 2, 2016, ISSN: 2045-2322. DOI: 10.1038/srep30550. URL: https://www.nature.com/articles/srep30550 (visited on 04/12/2024).

[40] D. B. MacManus and M. Ghajari, "Material properties of human brain tissue suitable for modelling traumatic brain injury," *Brain Multiphysics*, vol. 3, p. 100 059, 2022, ISSN: 26665220. DOI: 10.1016/j.brain.2022.100059. URL: https://linkinghub.elsevier.com/retrieve/pii/S2666522022000168 (visited on 11/17/2023).

[41] Cleveland Clinic. "Thyroid overview." (Jun. 7, 2022), URL: https://my.clevelandclinic.org/health/body/23188-thyroid (visited on 03/21/2024).

[42] H. Sung, J. Ferlay, R. L. Siegel, M. Laversanne, I. Soerjomataram, A. Jemal, and F. Bray, "Global cancer statistics 2020: GLOBOCAN estimates of incidence and mortality worldwide for 36 cancers in 185 countries," *CA: A Cancer Journal for Clinicians*, vol. 71, no. 3, pp. 209–249, May 2021, ISSN: 0007-9235, 1542-4863. DOI: 10.3322/caac.21660. URL: https://acsjournals.onlinelibrary.wiley.com/doi/10.3322/caac.21660 (visited on 03/02/2024).

[43] M. G. Lechner and J. M. Hershman, "Thyroid nodules and cancer in the elderly," in *Endotext*, K. R. Feingold, B. Anawalt, M. R. Blackman, *et al.*, Eds., South Dartmouth (MA): MDText.com, Inc., 2000. URL: http://www.ncbi.nlm.nih.gov/books/NBK278969/ (visited on 03/29/2024).

[44] American Thyroid Association (ATA), "Thyroid nodules," Brochure, 2018. URL: https://www.thyroid.org/thyroid-nodules/.

[45] "Overdiagnosis is a major driver of the thyroid cancer epidemic: Up to 50-90% of thyroid cancers in women in high-income countries estimated to be overdiagnoses," Lyons, France, Press Release, Aug. 18, 2016.

[46] R. Udelsman and Y. Zhang, "The epidemic of thyroid cancer in the united states: The role of endocrinologists and ultrasounds," *Thyroid*, vol. 24, no. 3, pp. 472–479, Mar. 2014, ISSN: 1050-7256, 1557-9077. DOI: 10.1089/thy.2013.0257. URL: https://www.liebertpub.com/doi/10.1089/thy.2013.0257 (visited on 03/02/2024).

[47] S. Vaccarella, S. Franceschi, F. Bray, C. P. Wild, M. Plummer, and L. Dal Maso, "Worldwide thyroid-cancer epidemic? the increasing impact of overdiagnosis," *The New England Journal of Medicine*, vol. 375, no. 7, pp. 614–617, Aug. 18, 2016, ISSN: 1533-4406. DOI: 10.1056/NEJMp1604412.

[48] L. Davies and H. G. Welch, "Current thyroid cancer trends in the united states," *JAMA otolaryngology– head & neck surgery*, vol. 140, no. 4, pp. 317–322, Apr. 2014, ISSN: 2168-619X. DOI: 10.1001/jamaoto.2014.1.

[49] S. Alshaikh, Z. Harb, E. Aljufairi, and S. A. Almahari, "Classification of thyroid fine-needle aspiration cytology into bethesda categories: An institutional experience and review of the literature," *CytoJournal*, vol. 15, p. 4, Feb. 16, 2018, ISSN: 0974-5963. DOI: 10.4103/cytojournal.cytojournal_32_17. URL: https://cytojournal.com/classification-of-thyroid-fine-needle-aspiration-cytology-into-bethesda-categories-an-institutional-experience-and-review-of-the-literature/ (visited on 02/27/2024).

[50] C. C. Juhlin and Z. W. Baloch, "The 3rd edition of bethesda system for reporting thyroid cytopathology: Highlights and comments," *Endocrine Pathology*, Nov. 30, 2023, ISSN: 1046-3976, 1559-0097. DOI: 10.1007/s12022-023-09795-9. URL: https://link.springer.com/10.1007/s12022-023-09795-9 (visited on 03/02/2024).

[51] L. Lan, Y. Luo, M. Zhou, L. Huo, H. Chen, Q. Zuo, and W. Deng, "Comparison of diagnostic accuracy of thyroid cancer with ultrasound-guided fine-needle aspiration and core-needle biopsy: A systematic review and meta-analysis," *Frontiers in Endocrinology*, vol. 11, p. 44, Feb. 13, 2020, ISSN: 1664-2392. DOI: 10.3389/fendo.2020.00044. URL: https://www.frontiersin.org/article/10.3389/fendo.2020.00044/full (visited on 03/05/2024).

[52] P. Trimboli, G. Treglia, L. Guidobaldi, *et al.*, "Detection rate of fna cytology in medullary thyroid carcinoma: A meta-analysis," *Clinical Endocrinology*, vol. 82, no. 2, pp. 280–285, Feb. 2015, ISSN: 0300-0664, 1365-2265. DOI: 10.1111/cen.12563. URL: https://onlinelibrary.wiley.com/doi/10.1111/cen.12563 (visited on 03/05/2024).

[53] A. D. Workman, S. Soylu, D. Kamani, *et al.*, "Limitations of preoperative cytology for medullary thyroid cancer: Proposal for improved preoperative diagnosis for optimal initial medullary thyroid carcinoma specific surgery," *Head & Neck*, vol. 43, no. 3, pp. 920–927, Mar. 2021, ISSN: 1043-3074, 1097-0347. DOI: 10.1002/hed.26550. URL: https://onlinelibrary.wiley.com/doi/10.1002/hed.26550 (visited on 03/05/2024).

[54] C. DiGennaro, V. Vahdatzad, M. S. Jalali, A. Toumi, T. Watson, G. S. Gazelle, N. Mercaldo, and C. C. Lubitz, "Assessing bias and limitations of clinical validation studies of molecular diagnostic tests for indeterminate thyroid nodules: Systematic review and meta-analysis," *Thyroid*, thy.2022.0269, Sep. 26, 2022, ISSN: 1050-7256, 1557-9077. DOI: 10.1089/thy.2022.0269. URL: https://www.liebertpub.com/doi/10.1089/thy.2022.0269 (visited on 03/05/2024).

[55] P. Trimboli, G. Treglia, L. Guidobaldi, *et al.*, "Clinical characteristics as predictors of malignancy in patients with indeterminate thyroid cytology: A meta-analysis," *Endocrine*, vol. 46, no. 1, pp. 52–59, May 2014, ISSN: 1355-008X, 1559-0100. DOI: 10.1007/s12020-013-0057-1. URL: http://link.springer.com/10.1007/s12020-013-0057-1 (visited on 03/05/2024).

[56] Sharon Reynolds. "Why have thyroid cancer diagnoses spiked for US women?" Cancer Currents Blog. (Sep. 28, 2021), URL: https://www.cancer.gov/news-events/cancer-currents-blog/2021/thyroid-cancer-diagnosed-more-in-women.

[57] S. Raayai-Ardakani, Z. Chen, D. R. Earl, and T. Cohen, "Volume-controlled cavity expansion for probing of local elastic properties in soft materials," *Soft Matter*, vol. 15, no. 3, pp. 381–392, 2019, ISSN: 1744-683X, 1744-6848. DOI: 10.1039/C8SM02142B. URL: http://xlink.rsc.org/?DOI=C8SM02142B (visited on 05/18/2023).

[58] S. Chockalingam, C. Roth, T. Henzel, and T. Cohen, "Probing local nonlinear viscoelastic properties in soft materials," *Journal of the Mechanics and Physics of Solids*, vol. 146, p. 104 172, Jan. 1, 2021, ISSN: 0022-5096. DOI: 10.1016/j.jmps.2020.104172. URL: https://www.sciencedirect.com/science/article/pii/S0022509620304026 (visited on 09/18/2023).

[59] J. A. Zimberlin, N. Sanabria-DeLong, G. N. Tew, and A. J. Crosby, "Cavitation rheology for soft materials," *Soft Matter*, vol. 3, no. 6, p. 763, 2007, ISSN: 1744-683X, 1744-6848. DOI: 10.1039/b617050a. URL: http://xlink.rsc.org/?DOI=b617050a (visited on 05/18/2023).

[60] C. W. Barney, C. E. Dougan, K. R. McLeod, *et al.*, "Cavitation in soft matter," *Proceedings of the National Academy of Sciences of the United States of America*, vol. 117, no. 17, pp. 9157–9165, 2020, Publisher: National Academy of Sciences, ISSN: 0027-8424. URL: https://www.jstor.org/stable/26929913 (visited on 09/18/2023).

[61] A. S. Mijailovic, S. Galarza, S. Raayai-Ardakani, N. P. Birch, J. D. Schiffman, A. J. Crosby, T. Cohen, S. R. Peyton, and K. J. Van Vliet, "Localized characterization of brain tissue mechanical properties by needle induced cavitation rheology and volume controlled cavity expansion," *Journal of the Mechanical Behavior of Biomedical Materials*, vol. 114, p. 104 168, Feb. 1, 2021, ISSN: 1751-6161. DOI: 10.1016/j.jmbbm.2020.104168. URL: https://www.sciencedirect.com/science/article/pii/S1751616120307104.

[62] Christine Roth, "Local probing and modelling of viscoelasticity in soft materials: Advanced volume controlled cavity expansion," Ph.D. dissertation, Massachusetts Institute of Technology (MIT), Mar. 15, 2020.

[63] B. M. Unikewicz, A. M. Pincot, and T. Cohen, *An accessible instrument for measuring soft material mechanical properties*, 2024. arXiv: 2404.15036 [physics.ins-det].

[64] W. P. I. (WPI), *Ump3 with micro2t/4t instruction manual*, 2016.

[65] T. R. Kucklick, "Chapter 3. introduction to needles and cannulae," in *The Medical Device R&D Handbook*, 2nd, Boca Raton: Taylor and Francis, Jan. 27, 2013, pp. 44–45, ISBN: 978-0-429-19154-1.

[66] S. Jiang, P. Li, Y. Yu, J. Liu, and Z. Yang, "Experimental study of needle–tissue interaction forces: Effect of needle geometries, insertion methods and tissue characteristics," *Journal of Biomechanics*, vol. 47, no. 13, pp. 3344–3353, Oct. 2014, ISSN: 00219290. DOI: 10.1016/j.jbiomech.2014.08.007. URL: https://linkinghub.elsevier.com/retrieve/pii/S002192901400431X (visited on 09/19/2023).

[67] M. G. Jushiddi, R. M. Cahalane, M. Byrne, A. Mani, C. Silien, S. A. Tofail, J. J. Mulvihill, and P. Tiernan, "Bevel angle study of flexible hollow needle insertion into biological mimetic soft-gel: Simulation and experimental validation," *Journal of the Mechanical Behavior of Biomedical Materials*, vol. 111, p. 103 896, Nov. 2020, ISSN: 17516161. DOI: 10.1016/j.jmbbm.2020.103896. URL: https://linkinghub.elsevier.com/retrieve/pii/S1751616120304501 (visited on 03/04/2024).

[68] M. Gumus, N. Cay, O. Algin, A. Ipek, R. Unlu Ersoy, O. Belenli, and S. Ugras, "Comparison of 21-g and 27-g needles for the sample adequacy in the aspiration biopsy of the thyroid nodules," *Diagnostic and Interventional Radiology*, 2011, ISSN: 1305-3825. DOI: 10.4261/1305-3825.DIR.4340-11.1. URL: http://cms.galenos.com.tr/Uploads/Article_56984/Diagn%20Interv%20Radiol-18-102-En.pdf (visited on 09/19/2023).

[69] A. Tanaka, M. Hirokawa, M. Higuchi, R. Kanematsu, A. Suzuki, S. Kuma, T. Hayashi, T. Kudo, and A. Miyauchi, "Optimal needle size for thyroid fine needle aspiration cytology," *Endocrine Journal*, vol. 66, no. 2, pp. 143–147, 2019, ISSN: 0918-8959, 1348-4540. DOI: 10.1507/endocrj.EJ18-0422. URL: https://www.jstage.jst.go.jp/article/endocrj/66/2/66_EJ18-0422/_article (visited on 02/20/2024).

[70] M. Mahvash and P. Dupont, "Mechanics of dynamic needle insertion into a biological material," *IEEE Transactions on Biomedical Engineering*, vol. 57, no. 4, pp. 934–943, Apr. 2010, ISSN: 0018-9294. DOI: 10.1109/TBME.2009.2036856. URL: http://ieeexplore.ieee.org/document/5339196/ (visited on 04/04/2024).

[71] F. Romack, C. Turner, and B. Day, "Anatomy of the porcine thyroid," *Research Bulletin (University of Missouri: Agricultural Experiment Station)*, no. 838, Nov. 1964. URL: https://mospace.umsystem.edu/xmlui/handle/10355/58114.

[72] M.-T. Lee and C.-Y. Wang, "Case experience of radiofrequency ablation for benign thyroid nodules: From an ex vivo animal study to an initial ablation in taiwan," *Journal of Medical Ultrasound*, vol. 24, no. 1, pp. 32–38, Mar. 2016, ISSN: 09296441. DOI: 10.1016/j.jmu.2016.03.003. URL: http://linkinghub.elsevier.com/retrieve/pii/S0929644116300054 (visited on 09/19/2023).

[73] M. Al Dawish, A. Alwin Robert, K. Al Shehri, S. Hawsawi, M. Mujammami, I. A. Al Basha, M. Alrasheed, S. Asiri, M. Alzouman, and E. Alkharashi, "Risk stratification of thyroid nodules with bethesda III category: The experience of a territorial healthcare hospital," *Cureus*, May 19, 2020, ISSN: 2168-8184. DOI: 10.7759/cureus.8202. URL: https://www.cureus.com/articles/32136-risk-stratification-of-thyroid-nodules-with-bethesda-iii-category-the-experience-of-a-territorial-healthcare-hospital (visited on 03/10/2024).

[74] A. Al-Azzawi and T. Takahashi, "Anatomical variations of the thyroid gland: An experimental cadaveric study," *Annals of Medicine and Surgery*, vol. 70, p. 102 823, Oct. 2021, ISSN: 20490801. DOI: 10.1016/j.amsu.2021.102823. URL: https://linkinghub.elsevier.com/retrieve/pii/S2049080121007731 (visited on 02/22/2024).

[75] L. Bhattarai, "Morphometric variations of thyroid gland: A cadaeric study," vol. 6, no. 2, 2023.